Atmospheric Environment 293 (2023) 119419

Contents lists available at ScienceDirect

Atmospheric Environment

journal homepage: www.elsevier.com/locate/atmosenv

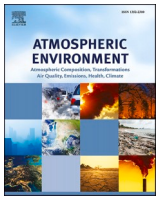

Effects of emission sources on the particle number size distribution of ambient air in the residential area

Sami D. Harni [a,*], Sanna Saarikoski [a], Joel Kuula [a], Aku Helin [a,1], Minna Aurela [a], Jarkko V. Niemi [b], Anu Kousa [b], Topi Rönkkö [c], Hilkka Timonen [a]

[a] Atmospheric Composition Research, Finnish Meteorological Institute, Helsinki, Finland
[b] Helsinki Region Environmental Services Authority (HSY), Helsinki, Finland
[c] Aerosol Physics Laboratory, Tampere University, Tampere, 33100, Finland

HIGHLIGHTS

- Events with a dominant particle source were identified systematically from ambient data.
- Particle sources were traffic, biomass combustion, biogenic and long-range transport.
- Number size distributions from different sources had different shapes.
- Traffic produced significantly smaller particles compared to wood combustion.
- Particle number size distribution from wood-burning showed large variability.

ABSTRACT

Particle size distribution is a major factor in the health and climate effects of ambient aerosols, and it shows a large variation depending on the prevailing atmospheric emission sources. In this work, the particle number size distributions of ambient air were investigated at a suburban detached housing area in northern Helsinki, Finland, during a half-year period from winter to summer of 2020. The measurements were conducted with a scanning mobility particle sizer (SMPS) with a particle size range of 16–698 nm (mobility diameter), and the events with a dominant particle source were identified systematically from the data based on the time of the day and different particle physical and chemical properties. During the measurement period, four different types of events with a dominant contribution from either wood-burning (WB), traffic (TRA), secondary biogenic (BIO), or long-range transported (LRT) aerosol were observed. The particle size was the largest for the LRT events followed by BIO, WB, and TRA events with the geometric mean diameters of 72, 62, 57, and 41 nm, respectively. BIO and LRT produced the largest particle mode sizes followed by WB, and TRA with the modes of 69, 69, 46, and 25 nm, respectively. Each event type had also a noticeably different shape of the average number size distribution (NSD). In addition to the evaluation of NSDs representing different particle sources, also the effects of COVID-19 lockdown on specific aerosol properties were studied as during the measurement period the COVID-19 restrictions took place greatly reducing the traffic volumes in the Helsinki area in the spring of 2020. These restrictions had a significant contribution to reducing the concentrations of NO_x and black carbon originating from fossil fuel combustion concentration, but insignificant effects on other studied variables such as number concentration and size distribution or particle mass concentrations (PM_1, $PM_{2.5}$, or PM_{10}).

1. Introduction

Particle size distribution is a key factor in the health and climate effects of ambient aerosols. For instance, the deposition of particles of inhaled air in the human respiratory tract depends strongly on the particle size, e.g. the ultrafine particles (diameter <100 nm) deposit efficiently deep in the lungs, into the vulnerable alveolar area (ICRP, 1994; Heyder, 2004). In addition, ambient aerosols affect the climate by cooling or warming it, depending on particle concentration, composition, and size that affect how aerosol particles scatter or absorb light (Pósfai and Buseck, 2010). When the particle size is large enough, they can affect indirectly the climate by acting as cloud condensation nuclei, with larger aerosol particle number concentrations leading to a higher number of smaller droplets increasing cloud albedo and cooling the climate (Twomey, 1977). The importance of particle size is also reflected in the latest WHO global air quality guideline (WHO, 2021) that

* Corresponding author. Erik Palménin aukio 1, 00560, Helsinki, Finland.
E-mail address: sami.harni@fmi.fi (S.D. Harni).
[1] Currently at Finnish Institute of Occupational Health, Helsinki, Finland.

https://doi.org/10.1016/j.atmosenv.2022.119419
Received 1 July 2022; Received in revised form 27 September 2022; Accepted 30 September 2022
Available online 12 October 2022

recommends measuring concentrations of ultrafine particles, as well as size segregated particle number concentrations in their new good practice statement. Furthermore, if standards for ambient particle number concentration measurements in the future are implemented, there is a need for a better understanding of particle number size distributions (NSDs) originating from different sources (Hopke et al., 2022).

Particle size depends strongly on the origin of particles. Sources of fine particles (<2.5 μm in diameter) in ambient air are typically highly heterogeneous but the main sources in urban areas are typically traffic, small-scale combustion in households, and secondary aerosol formation from biogenic and anthropogenic gases originating either from local, regional, or remote sources (Hovorka et al., 2015; Vargas et al., 2012; Saarikoski et al., 2008).

Traffic increases ambient particle concentrations in a wide particle size range, but especially in nanocluster, nucleation mode, and Aitken mode particle sizes (Birmili et al., 2009; Rönkkö et al., 2017; Hietikko et al., 2018; Enroth et al., 2016). In ambient air, the NSDs of traffic emissions consist typically of two or more particle modes (see e.g. Enroth et al., 2016; Pirjola et al., 2017). This is caused by different emissions of individual cars but also by various formation mechanisms of fresh exhaust particles. Engine exhaust particles are formed during the combustion of fuel and engine oil compounds, resulting in solid soot and ash particles, and, additionally, particles can be formed during the exhaust cooling and dilution processes in the atmosphere, resulting in a significant increase in fresh exhaust particle number; e.g. Kittelson et al. (2006) reported bimodal distribution for heavy-duty diesel engines with nucleation mode at 6–11 nm and accumulation mode at 52–62 nm in cruise and acceleration conditions on the highway. Karjalainen et al. (2014) made similar observations that a gasoline vehicle emitted nonvolatile exhaust particles consisting of two distinct modes, one at 10 nm and the other around 70 nm during acceleration and steady-state conditions using the New European Driving Cycle (NEDC), also several studies other have reported the mode of particles in sub 10 nm particle sizes (Rönkkö et al., 2007; De Filippo and Maricq, 2008; Sgro et al., 2008, 2012; Heikkilä et al., 2009; Kuuluvainen et al., 2020). Nuclei mode formation is strongly linked with the cooling dilution of exhaust and it is more often visible in the measurements made on road than in the laboratory measurements which are not always designed to mimic real-world semivolatile particle emission (Kittelson et al., 2006).

Another significant local pollution source in urban areas is biomass burning. Particularly in residential areas, wood-burning is used as a complementary heating method, heating sauna stoves, and decorative burning. Wood-burning has been shown to produce varying size distributions depending on the phase of the combustion efficient combustion and even the between different measurements from the same combustion phase. For example for efficient combustion multiple different particle sizes have been reported: Most particles being around 30–40 nm (Wardayo et al., 2006), geometric mean diameters (GMD) varying between 56 and 65 nm (Tissari et al., 2008), and mean particle size being 150 nm (Timonen et al., 2021). Similarly, varying particle sizes have been reported for smoldering conditions: 50–76 nm (Wardayo et al., 2006) and 2–2.5 GMDs compared to normal burning conditions (at 56–65 nm) (Tissari et al., 2008). Also, the number of modes varies between different studies. The NSDs can be either unimodal, (Wardayo et al., 2006), bimodal (Mustafa et al., 2017), or polydisperse (Tiwari et al., 2014).

Besides being emitted as primary particles, a substantial fraction of aerosols in urban areas originate from secondary particle formation, in which biogenic or anthropogenic vapors either condense on existing particles or form new particles (Kulmala, 2003; Rönkkö and Timonen, 2019; Petäjä et al., 2022). The formation of secondary organic aerosol is caused by the oxidation of volatile organic compounds (VOCs) in the atmosphere (Mahilang et al., 2021) while inorganic species sulfate, nitrate, and ammonium are mostly formed from inorganic precursor gases SO_2, NO_x, and ammonia. In highly polluted areas with high NO_x, particle number, and amine concentration, H_2SO_4-based nucleation is the primary form of new particle formation, while in less polluted suburban areas the contribution of organics is expected to be larger (Xiao et al., 2021).

The number of studies investigating particle NSDs originating from biogenic emissions is rather low. Using positive matrix factorization, Rivas et al. (2020) have found count median diameter (CMD) of 106.1 and 74.7 nm and modes of 100 and 99.9 nm for the biogenic particles in urban background and street canyon in Helsinki, respectively. Artaxo and Hansson (1995) have reported that biogenic emissions are the most important factor influencing the ambient particle concentrations under 0.25 μm particles in diameter, whereas larger particle sizes were dominated by mineral dust at the Amazon forest background station.

In addition to local sources, a significant fraction of particles in urban areas originates from particles transported from other areas. Hussein et al. (2014) have reported that Aitken (diameter 25–100 nm) and accumulation (0.1–1 μm) mode particles dominate long-range transport (LRT) and short-range transport (SRT) particle concentrations in the Helsinki area. Pirjola et al. (2017) detected a mode of number size distribution at 300 nm during a LRT event in Helsinki. Additionally, wildfires occasionally cause episodes in Finland increasing particle concentrations and particle size (60–250% compared to non-event days) (Saarikoski et al., 2007).

This study aims to systematically characterize NSDs during different prevailing sources in a Pirkkola suburban residential area, in Helsinki, Finland. Identified particle sources were residential wood-burning (WB), traffic (TRA), secondary biogenic (BIO), and long-range transport (LRT) aerosol. The sources were identified based on the particle chemical composition, time of day, temperature, and NO_x and $PM_{2.5}$ concentrations. In addition to NSDs related to the sources, the effects of COVID-19 lockdown on specific aerosol properties were studied, as, during the measurement period in spring 2020, the COVID-19 restrictions took place in the Helsinki area. Understanding the differences in the number size distributions related to various particle sources is crucial when the health and climate effects of particles need to be reduced. The contribution of different particle sources in ambient air has been changing in recent years and will be changed further in the future due to the regulations as well as citizen behavior.

2. Experimental

2.1. Measurement site

The measurements were conducted at the Pirkkola measurement site (60.234211N, 24.922591E) in Helsinki, Finland between 11.12.2019 and 12.06.2020. The measurement site resides in a suburban detached housing area, nearby a small lightly trafficked road. The distance to the closest main street is ~600 m from the measurement location, and the distance to other major roads is 1 km in the directions of West, North, and East (Teinilä et al., 2022). Most of the nearby houses use wood-burning in fireplaces for additional heating and sauna stoves, both of them typical habits for northern countries (Kukkonen et al., 2020). The measurement site is described in detail in Kuula et al. (2020) and Saarikoski et al. (2021). The largest single source of $PM_{2.5}$ and black carbon (BC) in Finland has been shown to be residential wood-burning contributing 37% and 55% of total emissions of these pollutants, respectively (Savolahti et al., 2016). In Helsinki, residential wood-burning has been estimated to contribute from 18 to 29% to $PM_{2.5}$ in urban and 31–66% in suburban areas, during the cold period (Saarnio et al., 2012). However, air quality in Finland is typically relatively good because of the rather low local emissions and regional urban background concentrations. That enabled us to investigate the impact and characteristics of individual sources in detail in this study.

2.2. Instruments

The sampling of ambient aerosol for the instruments was done at a height of 4 m from the ground without a size cut in the inlet. The air sample was drawn inside the measurement cabin with a fan, and the separate airflows for the individual instruments were taken from the main airflow. The NSDs were measured using a scanning mobility particle sizer (SMPS, TSI. Inc., USA) with a measurement size range of 15–698 nm and a time resolution of 3 min. The SMPS consisted of a differential mobility analyzer (DMA, model 3080, TSI Inc., USA) with a KR-85 neutralizer and a condensation particle counter (CPC, model 3775, TSI Inc., USA). The operation principle and response functions of the DMA are presented in Hoppel (1978). The SMPS operated with 1.5 L min^{-1} airflow. During the data analysis, the SMPS was found to measure particles in the three smallest particle size classes (14.6, 15.1, and 15.7 nm) inaccurately, and therefore, the size range of the SMPS was limited to start from 16.3 nm in this study. From the size distribution data measured with SMPS, also the total particle number concentrations for the measured size range were calculated. Additionally, total particle number concentrations were measured with a water-CPC (wCPC, Model 3789, TSI. Inc., USA) with a measurement range of 2–1000 nm.

BC concentrations were measured with an aethalometer (model AE33, Aerosol d.o.o, Slovenia; Drinovec et al., 2015). AE33 operated with a flow rate of 5 L min^{-1} and a time resolution of 1 min. The size cut of 1 μm for the AE33 was set by using a sharp cut cyclone (Model SCC1.197, BGI Inc., Butler, NJ, USA) in its inlet. Multiple scattering enhancement factor (C) of 1.57 was utilized (Drinovec et al., 2015) and default mass absorption coefficient values were used. BC was divided into BC originated from fossil fuel combustion (BC_{ff}) and wood-burning (BC_{wb}) by using the Aethalometer model (Sandradewi et al., 2008). The used Ångström exponents values for fossil fuel and wood-burning were 0.9 and 1.68, respectively (Zotter et al., 2017). The chemical composition (total organics (Org), sulfate (SO_4), nitrate (NO_3), ammonium (NH_4), chloride (Chl)) of PM_1 was measured with a Time-of-Flight Aerosol Chemical Speciation Monitor (ToF-ACSM, Aerodyne Research Inc., USA; Fröhlich et al., 2013). The time resolution of the measurements was approximately 11.5 min. Nitrogen oxides (NO_x) were measured with a Horiba APNA 370 (Kyoto, Japan), and particle mass concentration was measured with a GRIMM Aerosol Spectrometer (model 1.80, 31 channels, 0.25–32 μm) with a time resolution of 1 min using factory settings. The measured results from GRIMM were corrected to correspond to the EU-reference method using correction equations (Walden et al., 2017).

2.3. Meteorology

The meteorological data used in this study was attained from the Kumpula weather station, situated approx. 4 km southeast of the Pirkkola measurement site. The ambient temperature during the whole measurement period is presented in Fig. 1. During the measurement period, the average temperature was 4.8 °C, with the monthly average temperature varying between 0.9 °C (February) and 15 °C (June). It should be noted here that winter 2019–2020 was exceptionally warm in Helsinki with thermic winter lasting only 5 days between 25 and 29.2., and a 10-day moving average temperature remained during those days most of the time between 0 and 5 °C. The 10-day moving average temperature rose above 5 °C in 16.4., and remained there for the rest of the measurement period. Therefore, the measurement period naturally split into two different temperature periods: the cold period (11.12.2019–16.4.2020) and the warm period (17.4.2020–12.6.2020). The cold period was divided further into two periods, before and after COVID-19 restrictions, to evaluate the effects of the restriction period; without COVID-19 restrictions (w/o CR) (11.12.2019–15.3.2020) and the time of COVID-19 restrictions (CR) (16.3.2020–16.4.2020) (Fig. 1). The COVID-19 restrictions included e.g. closing schools and other public places, restricting recreational activities, strongly promoting remote working, and avoidance of crowded places. An important thing to note is that all the COVID-19 restrictions did not end by the start of the warm period but partly continued over the rest of the measurements. Therefore, the whole warm period was affected by the partial COVID-19 restrictions. Traffic volumes during workdays decreased in Uusimaa (a region in south Finland) by 38% due to the COVID-19 restriction compared to the last week before the implication of the restrictions (Finnish Trasport Infrastructure Agency).

2.4. Data analysis

Using source-specific selection criteria, four different types of events affecting the ambient aerosol at the measurement site were identified from the measurement data. These events are called in this study wood-burning (WB), traffic (TRA), secondary biogenic (BIO), and long-range transported (LRT) aerosol events. The events were extracted from 1-h average data based on the time of day, NO_x concentrations, and PM_1 (particles with diameter <1 μm) chemical composition. It should be noted that the criteria for the event identification were set so that only the events with a clear primary contribution from a single source were extracted but there was no exact limit for the contribution of the particular source to ambient concentrations. Therefore, the events only highlight the typical NSDs for different particle sources detected in urban areas with small contributions from other sources. The exact limit

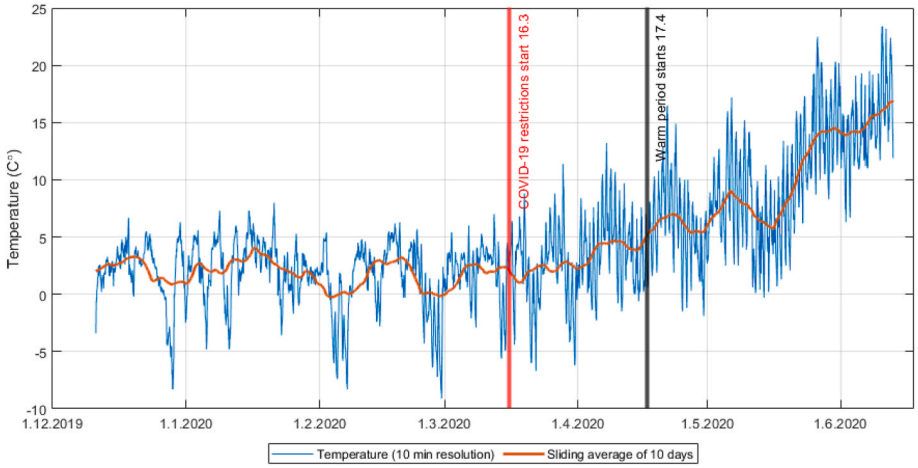

Fig. 1. Ambient temperature during the measurement period 11.12.2019–12.6.2020 (10-min resolution in blue and 10-day moving average value with an orange line). The division between cold and warm periods has been marked with a vertical black line. The cold period has been split into two parts before and after COVID-19 restrictions to evaluate their effect. The start of the COVID-19 restrictions is marked with a vertical red line. (For interpretation of the references to color in this figure legend, the reader is referred to the Web version of this article.)

values for the selection of events are described shortly below and also listed in the supplemental material (Table 1).

WB events were extracted from the data by using biomass burning fraction of BC (BB%) calculated by the Aethalometer model, and the fraction of *m/z* 60 in total organics (*f*60) in the ToF-ACSM data. The m/z 60 is an organic ion fragment that originates from levoglucosan which is emitted in large quantities in biomass burning and can therefore be used as a fresh biomass burning indicator (Simoneit et al., 1999; Saarnio et al., 2012). The criteria for WB was that BB%, *f*60, and total BC and organics needed to exceed the 80th percentile values observed during the measurement period. WB events were only searched within a time window of 18.00–03.00. This time window was selected based on the diurnal variation of BB% presented in the supplement (Fig. S1), and previous publications that have indicated that the emissions from the fireplaces and saunas are largest during the evening hours (Helin et al., 2018; Saarikoski et al., 2021).

For TRA events, the ion fragment of m/z 57 was selected as the marker for traffic as alkyl ($C_nH_{2n+1}^+$) and alkene ($C_nH_{2n-1}^+$) fragments have been related to vehicle exhaust in previous studies (Zheng et al., 2020). For TRA events, ambient NO_x concentration and the fraction of *m/z* 57 in total organics (*f*57) were required to exceed 80th percentile values and BB% could not exceed the 20th percentile value during the measurement period. BC and organics were not likely to be strongly elevated during the TRA events as the measurement site resides relatively far from the busy roads and the highest concentrations of organics and BC are likely to be related to WB, but these values are still expected to be at least slightly increased. Therefore, to ensure the reliability of BB % and *f*57 fractions, the total BC and organics were required to exceed 50th percentile values. TRA events were only searched between morning rush hours of 06.00–10.00 when traffic flows are high. Also, the diurnal variation of NO_x (Fig. S2) was taken into account for choosing this time range.

The main criteria for the BIO events were that the hourly average temperature needed to exceed 15 °C. The temperature has been shown to impact the release of biogenic volatile compounds (BVOC) precursors such as isoprene that impacts the formation of biogenic secondary organic aerosol (BSOA) (Zhu et al., 2018). To ensure that other sources had only a minor influence on the particle properties during the BIO events, sulfate (mostly from LRT, see below), total BC, and NO_x were required to be below the 50th percentile.

Sulfate and $PM_{2.5}$ were selected as indicators for the LRT events as sulfate is typically a long-range transported species in the Helsinki area (Timonen et al., 2008; Aurela et al., 2015), and during the long-range transportation events, the $PM_{2.5}$ is also typically elevated (Niemi et al., 2009). Moving 24-h averages of both sulfate and $PM_{2.5}$ were required to exceed 80th percentile values of the measurement period during the LRT events. All LRTs that were shorter than 24 h were also removed to ensure that the high sulfate and $PM_{2.5}$ concentrations were not from the local sources.

The average size distributions were calculated only for the events that included full coverage of the SMPS data. Also, the chemical compositions of PM_1 were analyzed during these events to study the differences between the particle chemical composition for different sources. The observed number of events with the full coverage of the SMPS data were 24, 10, 12, and 3, and the total duration of 42, 15, 39, and 116 h for WB, TRA, BIO, and LRT events, respectively. For the statistical analysis of the size distributions, the GMD was calculated. Additionally, mode referring to the bin with the highest concentration of particles is used in this article to describe the NSD.

Three-day backward trajectories at 500 m arrival height (AGL) were calculated during the selected LRT events using the HYSPLIT back trajectory model (Stein et al., 2015) to identify the main source of aerosol. These trajectories are presented in the supplement (Figs. S3–5).

As the event identification is based on percentiles of different compounds it would be in principle possible to have a significant background from one single source during all the times that would dominate also the NSDs from other sources. However, the source apportionment has been studied earlier in a number of studies in Helsinki (e.g. Saarikoski et al., 2008; Timonen et al., 2008 and Chen et al., 2022) and the air in the Helsinki area is fairly clean making this kind of scenario of a constant background source unlikely especially during longer periods.

Table 1
Detection criteria for different event types (WB, TRA, BIO and LRT). Pctl = percentile, d = day, any means that parameter was not included in selection criteria.

	WB	TRA	BIO	LRT
Total BC (μg m^{-3})	>0.636 (80th pctl.)	>0.270 (50th pctl.)	<0.270 (50th pctl.)	any
BB (%)	>55.0 (80th pctl.)	<34.0 (20th pctl.)	any	any
f60	>0.0063 (80th pctl.)	any	any	any
f57	any	>0.0244 (80th pctl.)	any	any
Temperature	any	any	>15°	any
Duration (d)	any	any	any	>1
NO_x (μg m^{-3})	any	>14.6 (80th pctl.)	<6.26 (50th pctl.)	any
SO_4 (μg m^{-3})	any	any	<0.152 (50th pctl.)	1d sliding average > 0.410 (80th pctl.)
$PM_{2.5}$ (μg m^{-3})	any	any	any	1d sliding average > 5.93 (80th pctl.)
Total Org (μg m^{-3})	>1.79 (80th pctl.)	>0.677 (50th pctl.)	any	any
Time of day	18–03	06–10	any	any

3. Results and discussions

3.1. General description of concentrations during the measurement period

The hourly average values of the total particle number concentration measured with SMPS (16–698 nm) and wCPC (2–1000 nm), PM_{10}, $PM_{2.5}$, PM_1 components, NO_x, BC, BC_{ff}, and BC_{wb} were divided into cold, warm, w/o CR, and CR periods. Average values for these periods are listed in Table 1. The total particle number concentration was larger during the warm period than during the cold period, the difference being more significant to 16–698 nm particles measured with the SPMS than to 2–1000 nm particles measured with the wCPC. In general, the PN concentrations measured with the wCPC in the residential area were significantly higher (~39%) than the concentrations measured with the SMPS indicating that a significant portion of the particles was in the size range of 2–16 nm at the residential site. This is important considering the GMDs reported for different event types in chapter 3.3, as now the GMDs might significantly be larger than they would be if particle sizes starting from 2 nm would be included. However, the modes of different NSDs should not be affected unless the mode is the 16 nm limit.

In terms of chemical species, most of the species had larger mass concentrations during the cold period than during the warm period, except organics and sulfate which had 53 and 13% larger concentrations in the warm period compared to those in the cold period, respectively. PM_1 chemical composition in the cold period was relatively similar to the winter and warm period to summer in the Helsinki street canyon reported by Barreira et al. (2021). The most significant difference was the larger fraction of black carbon during wintertime (25% of PM_1 in this study) compared to the street canyon site (18% in Barreira et al., 2021). At the residential site in Pirkkola, the fraction of BC originated from biomass burning was roughly 50% whereas at the street canyon site it was much smaller, roughly 20% (Barreira et al., 2021). Regarding concentrations, slightly higher BC_{ff} concentrations have been reported for the other residential house areas in Helsinki on weekdays (0.49 ± 0.75 μg m^{-3}) and weekends (0.45 ± 0.72 μg m^{-3}), and BC_{wb} of 0.35 ±

0.68 μg m^{-3} for weekdays and 0.44 ± 0.90 μg m^{-3} for weekends (Helin et al., 2018) when compared to the Pirkkola residential site; BC_{ff} values of 0.33 ± 0.50 and 0.19 ± 0.21 and BC_{wb} values of 0.28 ± 0.48 and 0.15 ± 0.17 μg m^{-3} for cold and warm periods respectively. Overall, BC concentrations from 0.67 to 2.64 μg m^{-3} have been measured at traffic sites, 0.16 to 0.48 μg m^{-3} at the regional background sites, 0.64–0.80 μg m^{-3} in detached housing areas, and 0.42–0.68 μg m^{-3} at urban background stations in the Helsinki area (Luoma et al., 2021). Lower BC concentrations in Pirkkola can be largely a result of the combined effects of restrictions related to COVID-19 and the unusually warm winter of 2020 (Table 1). However, the contribution of BC in PM_1 (25 and 14% for cold and warm periods, respectively) was significantly higher when compared to Asia or South America where BC contribution in urban areas is typically well below 10% of fine PM (Gani et al., 2019; Reyes et al., 2021). The effect of COVID-19 on air quality parameters is presented later.

The average PM_{10} and $PM_{2.5}$ concentrations were significantly lower in Pirkkola during both the cold and warm periods (PM_{10}: 10.3 ± 11.0–8.7 ± 4.5 μg m^{-3} and $PM_{2.5}$ 4.9 ± 3.9–3.6 ± 1.9 μg m^{-3}, Table 1) compared to the values of 16 and 9.1 μg m^{-3} measured for PM_{10} and $PM_{2.5}$, respectively, in the Helsinki city center between 2013 and 2015 (Teinilä et al., 2019) or $PM_{2.5}$ (7.2 μg m^{-3}) measured at the street canyon site in Helsinki in 2015–2019 (Barreira et al., 2021). NO_x concentrations in Pirkkola (12.7 ± 20.6 and 7.3 ± 8.1 μg m^{-3} for cold and warm periods respectively, Table 1) were also relatively low compared to the hourly-averaged value of 76 μg m^{-3} for the traffic site in the Helsinki city center (Teinilä et al., 2019). Observed NO_x concentrations at Pirkkola compare better to the concentration of 8.5 μg m^{-3} measured at the Luukki rural site in the Helsinki Metropolitan area (64°53′N, 25°50′E) (Teinilä et al., 2019). This underlines that the Pirkkola is primarily a residential area and only secondarily under the influence of traffic emissions.

To study the effects of the COVID-19 restrictions on ambient concentration, the w/o CR and CR periods were compared. It was noticed that the concentrations of NO_x, BC, and especially BC_{ff} decreased during the COVID-19 restrictions with a reduction of 36, 19, and 24%, respectively (Table 2). In contrast, PM_{10}, $PM_{2.5}$, and total number concentrations increased slightly during the CR period. Globally, NO_2 concentrations were reduced by 34% which is higher than the reduction of 23% measured at Pirkkola (Torkmahalleh et al., 2021). Torkmahalleh et al. (2021) also reported a reduction of 15% for $PM_{2.5}$ during COVID-19 restrictions while in Pirkkola $PM_{2.5}$ concentrations increased. Notably, some of the differences in results might be the result of different analysis methods as in this study the COVID-19 restriction period was compared to the time period just before when for example Sokhi et al. (2021) compared the COVID-19 restriction period to the same time period of the previous years. Overall, the effects of the COVID-19 restrictions were found to be relatively small with respect to other components than NO_x as some of the decreasing BC concentrations could also be related to decreasing amount of wood-burning as the ambient temperature was slightly warmer during the COVID-19 restrictions compared to the w/o CR period. It should be noted that the comparison did not take into account any differences in meteorology (e.g. temperature, air mass origins) between the periods, or if the differences were caused by normal temporal variation outside the COVID-19 restrictions. Also, the concentrations of NO_x are generally low in Pirkkola and the NO_x and BC concentrations have been declining in the Helsinki area in recent years (Luoma et al., 2021). The reduction of ambient NO_x concentrations due to the COVID-19 restrictions has been reported e.g. by Liu et al. (2021), Bar et al. (2021), and Torkmahalleh et al. (2021).

3.2. Diurnal variation of particle number concentrations

Diurnal variations of particle number concentrations were investigated in respect of number size distributions. Fig. 2 shows the average particle number concentrations in terms of GMDs of NSDs (marked with colors) calculated for cold, warm, w/o CR, and CR periods with workdays and weekends separated. During the cold period, particle concentration peaked in the morning and late evening hours on workdays. The GMD of particles was smaller and the number concentration was higher in the morning peak compared to the evening peak. This can be related to the morning rush hour producing a significant amount of small particles. In the evening, the rise of particle concentrations was likely to be caused by residential wood-burning in the area. Similar higher particle number concentrations during the evening because of residential wood-burning have been reported in Northern Sweden by Krecl et al. (2008). The higher contribution of wood-burning can be seen in the diurnal trend of BC related to fossil fuel and biomass burning presented in the supplemental material (Fig. S6). Similar trends for particle number concentrations have been observed also in Fresno, California, in an area that is influenced by traffic, heating, cooking, and agriculture. They observed in wintertime, that particle number concentrations peaked during morning hours (6 a.m.–9 a.m.) and evening hours (5 p.m.–11 p.m.) with the highest GMDs between 6 p.m. and 5 a.m. (Watson et al., 2006). In this study, during the weekends, the morning traffic peak was still visible, but significantly smaller, whereas the evening peak likely caused by biomass combustion was significantly larger and entailed larger particles. The larger particle size was likely to be a result of the smaller contribution of traffic to the particle number concentrations. Overall the particles were larger at weekends compared to workdays during the cold period with an average hourly GMD of 57.4 nm and 52.7 nm at weekends and workdays, respectively. Similar observations on larger particle size during weekend evenings caused likely by residential wood-burning, have been made e.g. by Krecl et al. (2008).

Table 2
Average PM_{10}, $PM_{2.5}$, NO_x, NO, NO_2, BC, BC_{ff}, BC_{wb}, and particle number (PN) concentrations and standard deviation for the different periods; Cold (11.12.2019–16.4.2020), Warm (17.4–12.6.2020), without COVID-19 restrictions (w/o CR) (11.12.2019–15.3.2020), and during COVID-19 restrictions (CR) (16.3–16.4.2020). Values measured from PM_1 are marked with "*" as BC and other components with PM_1 were measured with different instruments and they had slightly different data coverages. Therefore, the total analyzed PM_1 and Org/BC have been calculated only for the periods during which both instruments were measuring, and individual components had been averaged over all the available data to get the best representatives of the period.

Component	Cold	Warm	w/o CR	CR
PN (16–698 nm) (cm^{-3}) SMPS	2900 ± 2400	3600 ± 1800	2700 ± 2600	3300 ± 1900
PN (2–1000 nm) (cm^{-3}) wCPC	5400 ± 4200	6100 ± 4100	5300 ± 4400	5600 ± 3700
PM_{10} (μg m^{-3})	10.3 ± 11.0	8.7 ± 4.5	9.6 ± 11.0	12.2 ± 10.7
$PM_{2.5}$ (μg m^{-3})	4.9 ± 3.9	3.6 ± 1.9	4.9 ± 3.8	5.1 ± 4.3
NO_x (μg m^{-3})	12.7 ± 20.6	7.3 ± 8.1	14.0 ± 21.9	9.0 ± 15.2
NO (μg m^{-3})	1.7 ± 9.1	0.2 ± 1.5	2.1 ± 9.7	0.50 ± 6.7
NO_2 (μg m^{-3})	10.1 ± 9.3	6.9 ± 6.7	10.7 ± 9.9	8.2 ± 7.3
PM_1 Composition				
Total analyzed PM_1	2.4 ± 2.7*	2.4 ± 1.6*	2.4 ± 2.6*	2.5 ± 2.9*
BC (μg m^{-3})	0.59 ± 0.93*	0.34 ± 0.37*	0.62 ± 1.01*	0.50 ± 0.64*
BC_{ff} (μg m^{-3})	0.31 ± 0.50*	0.19 ± 0.21*	0.33 ± 0.55*	0.25 ± 0.31*
BC_{wb} (μg m^{-3})	0.28 ± 0.48*	0.15 ± 0.17*	0.29 ± 0.51*	0.25 ± 0.36*
NH_4 (μg m^{-3})	0.19 ± 0.27*	0.14 ± 0.11*	0.18 ± 0.24*	0.20 ± 0.35*
Chl (μg m^{-3})	0.03 ± 0.03*	0.01 ± 0.01	0.03 ± 0.03*	0.03 ± 0.03*
NO_3 (μg m^{-3})	0.39 ± 0.60*	0.15 ± 0.15*	0.36 ± 0.45*	0.44 ± 0.87*
Org (μg m^{-3})	0.98 ± 1.17*	1.5 ± 1.2*	0.92 ± 1.08*	1.1 ± 1.4*
SO_4 (μg m^{-3})	0.24 ± 0.27*	0.27 ± 0.21*	0.25 ± 0.29*	0.19 ± 0.19*
Org/BC	2.2 ± 1.4*	5.3 ± 3.6*	2.0 ± 1.2*	2.8 ± 1.7*

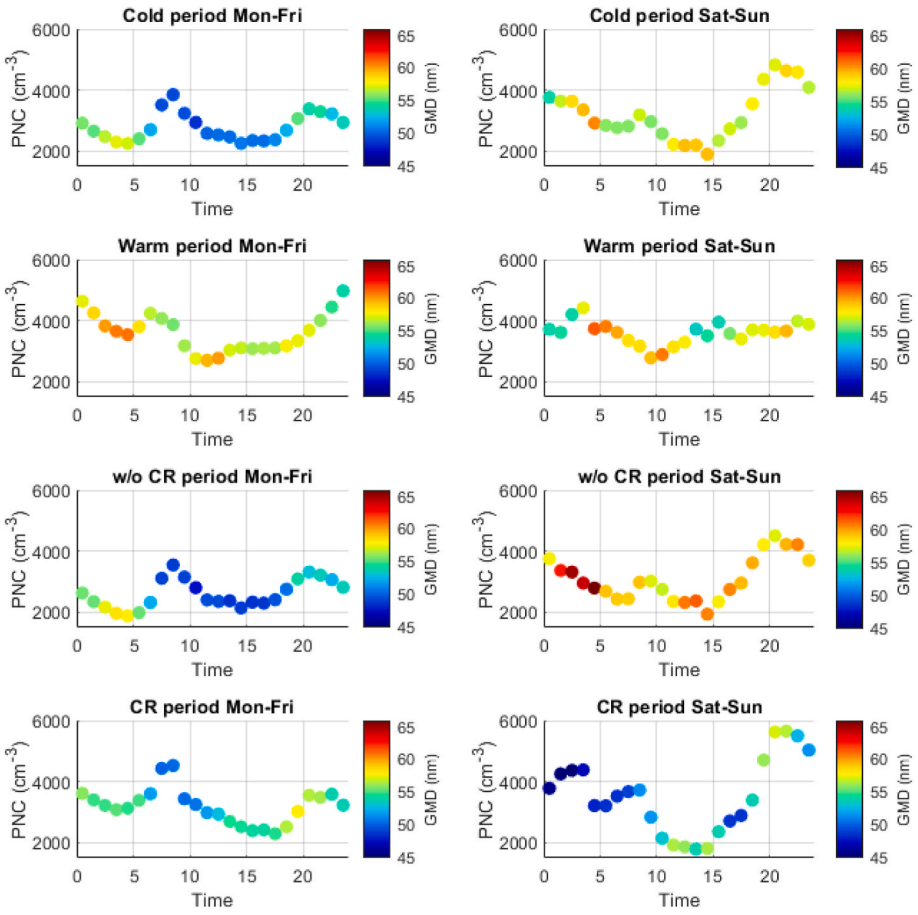

Fig. 2. Diurnal patterns of ambient air particle number concentrations (PNC) (16–698 nm) divided into workdays and weekends for cold, warm, and without COVID-19 restrictions (w/o CR) and COVID-19 restrictions (CR) periods. The geometric mean diameter (GMD) of particles is indicated with the color scale. The results are shown as 1 h averages. (For interpretation of the references to color in this figure legend, the reader is referred to the Web version of this article.)

During the workdays of the warm period, the diurnal pattern of particle number concentrations (PNC) was quite similar to the cold period. However, the rush hour peak in the morning was less pronounced, and the particle sizes were generally larger during the day although the particle number concentrations were alike. Quite surprisingly, the largest particle number concentrations were measured in the evening and night in the warm period. The larger particle sizes and the less pronounced morning peak can be related to the lower contribution of traffic to the total particle concentrations as the whole warm period was influenced to some degree by the COVID-19 restrictions that reduced traffic volumes even 38.4% (Finnish Transport Infrastructure Agency). The effects of the reduction in traffic volume are also supported by the reduction in ambient NO_x concentrations (Fig. S7). During weekends, the concentration peak during the morning rush hour or the evening hours was not visible. Notable from Fig. 2 is also that the largest particles were observed in the early morning around 5 o'clock during both cold and warm periods. This can be related to a lower amount of particle emissions during early morning hours and therefore larger contribution of aged background and LRT aerosols.

The diurnal patterns during workdays were similar both for w/o CR and CR periods, with w/o CR having slightly lower concentrations and smaller particle sizes. During weekends, the shapes of the diurnal patterns were very similar with a small morning peak likely related to traffic and a significantly larger evening peak related to residential combustion. However, the particle sizes were significantly larger during w/o CR, but these results might be affected by the relatively short duration of the CR period (4 weeks).

3.3. Number size distributions of different event types

Four different major sources of submicron particles (WB, TRA, BIO, LRT) were identified from the data and were selected for a closer examination. A total of 24 WB events were detected in Pirkkola lasting for a total of 43 h and covering 1.34% of the measurement period. WB events had a broad average NSD with a GMD of 57 nm, geometric standard deviation (GSD) of 2.0, and peak particle size (mode) at 46 nm (Fig. 3a). A large portion of these particles were likely soot particles in particle sizes smaller than approximately 50 nm. WB event particle size distributions showed a large variety of concentrations, especially in the particle sizes around 40 nm. The reason for the large variation might be an indication of poorly controlled combustion processes and varying combusted materials leading to more varying emission profiles for the WB events in comparison to other more tightly regulated combustion sources, such as engine emissions (see TRA events). Another factor causing variation is local meteorology affecting how the flue gas plumes reached the measurement site. GMD of the WB events was similar to those reported earlier for the conventional masonry heaters with GMD of 63 and 56 nm for firing and combustion phases in normal conditions, respectively, in laboratory measurements (Tissari et al., 2008). A significantly larger GMD of 123 nm for the firewood-burning emissions has been reported by Tiwari et al., (2014). Also, Tissari et al. (2008) have reported a significantly larger GMD of 230 nm for the combustion of wood in smoldering conditions. Hosseini et al. (2010) reported mode particle sizes of 29–52 nm for the cycle-averaged distributions of biomass burning particles. In atmospheric measurements, a modal size of 67 nm for aerosols related to wood-burning emissions has been

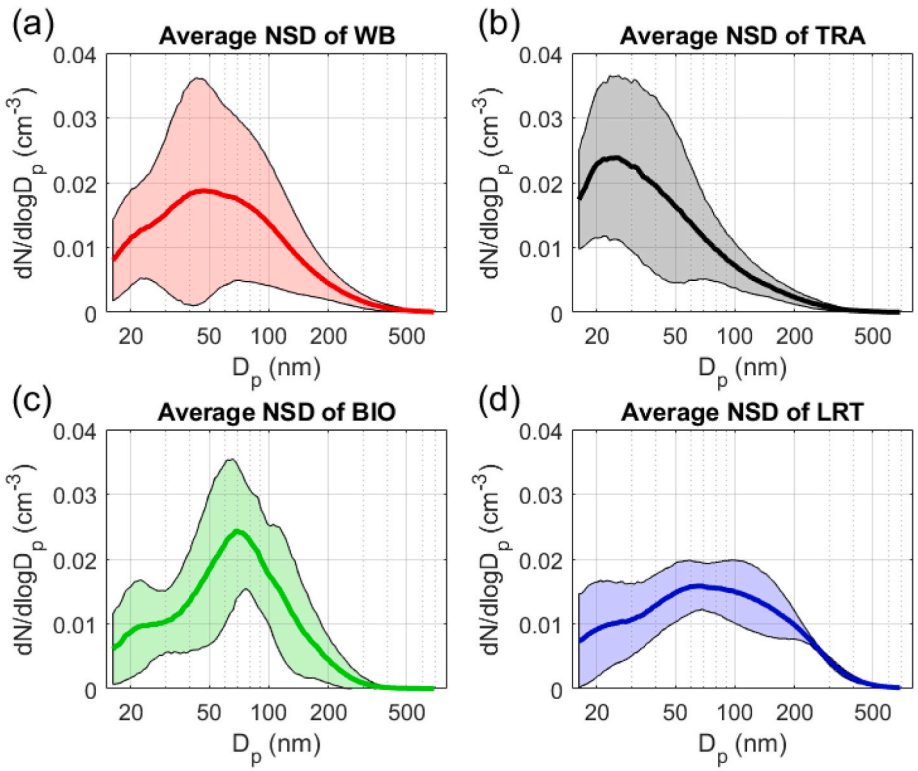

Fig. 3. Ambient air particle number size distributions for wood-burning (WB) (a), traffic (TRA) (b), secondary biogenic (BIO) (c), and long-range transport (LRT) (d) events. Average size distributions have been marked with bold lines and light-colored areas display standard deviations.

reported by Krecl et al. (2008), and the dominant evening mode with a peak particle size of 80 nm has been suggested as being from a non-traffic source likely residential wood-burning in Hering et al. (2007).

A total of 10 TRA events fulfilling the selection criteria and lasting for a total of 15h (0.47% of the measured data) were identified based on the selection criteria. The low number of traffic events is likely a result of the location of the measurement station in a residential area with the nearest heavily trafficked roads being situated some distance away. The average NSD of the TRA events is presented in Fig. 3b. The particle size during the TRA events was significantly smaller (particle GMD 41 nm with GSD of 1.9 and mode at 25 nm) compared to the WB events (Fig. 3b). NSD of the TRA events had also only one clear peak around the mode particle size with a long tail towards the larger particle sizes with very few particles larger than 200 nm (2.3% of particles at sizes 201.7–685.4 nm). NSD of the TRA events had the largest ultrafine particle fraction (<100 nm) at the measured size range (89.1%), compared to the fractions of 78.5, 76.6, and 64.0% for WB, BIO, and LRT, respectively (Fig. 3b). This might be because of the larger contribution of soot mode particles to the total NSD causing the highest concentration of small particles. The strong contribution of traffic emissions to ultrafine particle concentrations has been observed in several studies (Rönkkö and Timonen, 2019). Zhu et al. (2002) have reported a mode particle size of 38.8 nm 300 m downwind from the freeway, and slightly smaller particle sizes have been reported for traffic in the urban background with 22.9 nm in GMD and a mode particle size of 22.4 nm (Rivas et al., 2020).

EU legislation on vehicle particle number emissions controls solid particles with diameters larger than 23 nm (Euro 5b and 6 for diesel vehicles and Euro 6 for gasoline vehicles). However, a large fraction of particles observed during the TRAs were smaller than 23 nm as the mode particle size was as small as 24 nm, and the ten smallest particle size bins ranging between 16.3 and 22.5 nm included 21.1% of the particles. Also, the difference between the concentrations measured with wCPC and SMPS indicates that there was a significant number of particles in the particle sizes smaller than 16 nm during the whole measurement period as the hourly averaged total number concentrations measured with the wCPC were 39.2 ± 24.5% higher than the concentrations measured with the SMPS. Traffic has also been related to significant nanocluster aerosol emissions (<3 nm) (Hietikko et al., 2018; Rönkkö et al., 2017). Also, the contribution of semivolatile compounds may lead to the concentration near the detection limit to be a lower estimation. The figure showing the correlation between the wCPC and SMPS measurements is shown in the supplemental material (Fig. S8).

Overall 12 BIO events with the full SMPS data coverage lasting for a total of 39 h (1.21% of the available data) were identified from the data. For the BIO events, the average GMD was 62 nm (Fig. 3c) with a GSD of 1.9 and mode of 69 nm. Notable is a sharp peak in the particle size distribution around the mode particle size at 69 nm. The statistical values for the BIO events were smaller compared to the ones calculated at the Helsinki street canyon (74.7 nm (GDM) and 99.9 nm (mode)) and urban background (106.7 nm (GMD) and 100 nm (mode)) using a positive matrix factorization (Rivas et al., 2020). The measured GMDs were larger for the BIO events than for the WB and TRA events. Virtanen et al. (2010) have reported OH-initiated products of pine emissions with a peak particle concentration at 100 nm while O_3-initiated oxidation produced particles with a peak particle size of 28 nm.

A total of 3 long-range transport events lasting a total of 116h (3.60% of the available data) were extracted from the data. Notable is that, even though the number of events was small, these events lasted 116 h in total. The average GMD of LRT events was 72 nm with a GSD of 2.2 and mode at 69 nm (Fig. 3c). LRT had the highest GMD of the event types but the mode is at the same particle size as for the BIO events. This is likely to be caused by the relatively high contribution of particles from other sources that are mixed with the LRT particles. Therefore, defining the pure shape of the LRT events using this method is difficult. This is true also for the other event types but to less of an extent. In general, relatively large mode sizes of 90–120 nm have been associated with aged

polluted air masses in the earlier publications (Birmili and Harrison, 2008). The particle sizes in the accumulation mode (100–1000 nm) have the longest lifetimes in the atmosphere because of the least effective removal mechanism (Kwon et al., 2020). Therefore the mode particle size and GMD of LRT particles would have been expected to be in the larger particle sizes. In our study, the LRT also had the widest NSD, which is seen as the highest GSD. A significant difference between the LRT and other event types was also the relatively high number of particles in the size range of 201.7–685.4 nm, the contribution being 11.5, 2.3 4.8, and 3.2% for LRT, TRA, WB, and BIO, respectively. Notable is also a very small standard deviation of the NSD in particle sizes larger than 200 nm indicating that the concentrations and shapes of the distributions in particle sizes larger than 200 nm are very similar between different LRT events, which suggests that the particles larger than 200 nm were mostly from the LRT source or regional background with a minimal contribution from the local sources.

The ambient number size distributions have been studied in the Helsinki area e.g. by Rivas et al. (2020) and Pirjola et al., (2017). Rivas et al. (2020) studied number size distributions from two measurement sites, One traffic, and one urban background measurement site, and the source apportioned the data using positive matrix factorization (PMF). Pirjola et al., (2017) conducted a mobile lab with Sniffer van measurements during the winter of 2012 while driving around Helsinki metropolitan area. In contrast, in this study, the stationary measurements were performed in a detached housing area over a half-year measurement period and the events were detected based on the novel criteria. Also, the reported types of aerosol are different because of the measurement locations and methods. Pirjola et al. (2017) characterize size distributions for aerosol citya, highway, residential combustion, and background aerosol, and Rivas et al., (2020) report NSDs for photonucleation, traffic nucleation, fresh traffic, urban biogenic, and secondary aerosols.

3.4. Chemical composition of particles during different event types

The chemistry of PM_1 was investigated to elucidate further the characteristics of particles detected from different event types. During the WB events, PM_1 consisted of organic compounds (54%) and BC (34%) with other components having smaller contributions (Fig. 4). The fraction of BC was three times higher during the WB events than the average BC fraction measured at the Helsinki city center (Teinilä et al., 2019). However, the high mass concentration of BC, and especially BC_{wb}, were expected as they were used as criteria for the WB events. The ratio of organics to BC was 1.6 for an average event. This ratio has been shown to depend e.g. on the burning phase and aging varying between 0.27 and 4.48 with the ratio generally being higher for the aged aerosol (Timonen et al., 2021). Overall the high BC concentration in the WB events indicates a strong presence of soot mode in the WB size distribution which is also seen in Fig. 3a.

During the TRA events, the contributions of organics (39%) and BC (33%) to PM_1 (Fig. 4) were at a similar level. This is somewhat in agreement with Charron et al. (2019) who measured elemental carbon (EC) and organic carbon (OC) to have the same levels of concentrations of PM_{10} at a traffic measurement site. The ratio of organics to BC has

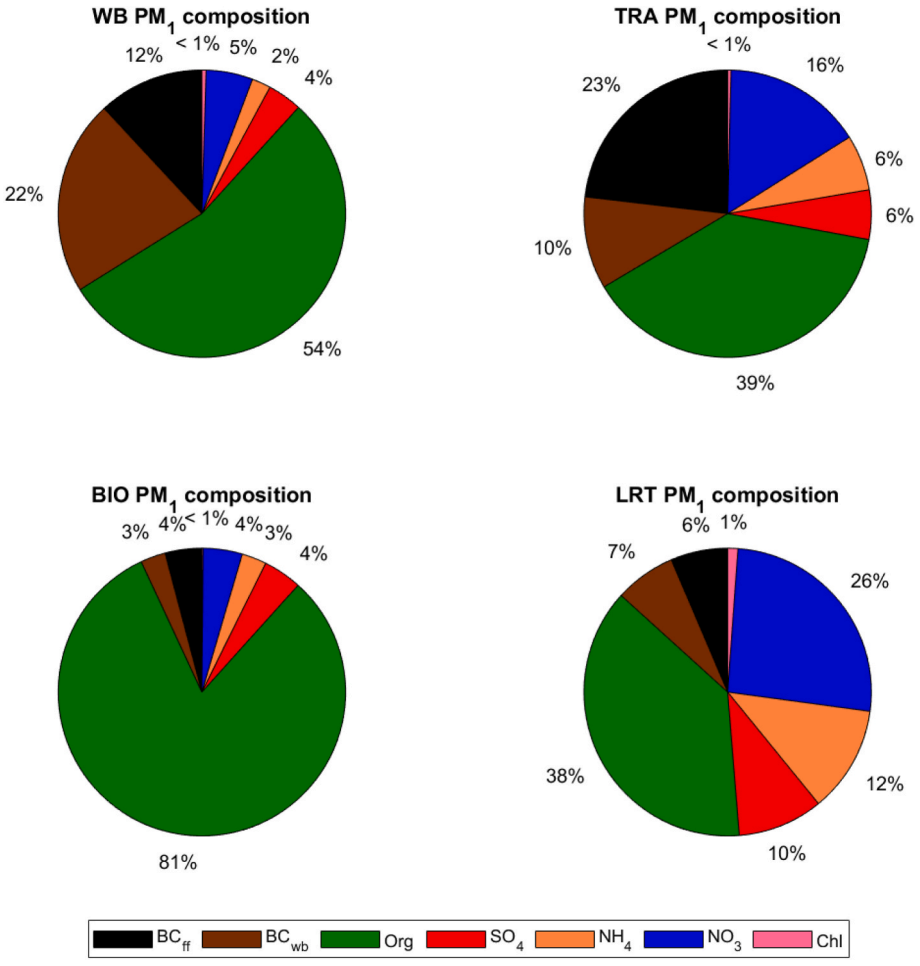

Fig. 4. Average PM_1 composition during the different event types: wood-burning(WB), traffic (TRA), secondary biogenic (BIO), and long-range transport (LRT). Organics (Org), sulfate (SO_4), ammonium (NH_4), nitrate (NO_3), and chloride (Chl) were measured with the ToF-ACSM and BC originated from fossil fuel combustion (BC_{ff}) and wood-burning (BC_{wb}) with the AE33.

been measured to be roughly 0.58–1.34 on highways in Helsinki (Enroth et al., 2016). The relatively high BC mass fraction of PM_1 with the high amount of BC_{ff} was expected as these are used as detection criteria for the TRA events. In addition, nitrate was elevated in PM_1 which has been also related to traffic emissions (Kim, 2019). Traffic has a significant BC fraction that is likely to cause the significant soot mode in the TRA NSD seen in Fig. 3b.

During the BIO events, 81% of the particulate matter consisted of organic compounds (Fig. 4) with only minor contributions from the other analyzed components. This supports the assumption of a biogenic source for these events. The average PM_1 concentration for the observed BIO events was 2.2 ± 1.3 μg m^{-3} with 1.8 ± 1.2 μg m^{-3} organics which was at a similar level as exceptionally high biogenic concentrations of 1.7 μg m^{-3} observed in Hyytiälä boreal research station in submicron particles (Corrigan et al., 2013). The chosen events mainly originated from biogenic sources as seen in the low contribution of inorganic components and BC, but we note that ambient aerosol always contains a variable fraction of particles from different sources.

During the LRT events, the mass fractions of inorganic species, sulfate, nitrate, and ammonium were the largest of all event types (Fig. 4). However, the fraction of sulfate (10%) was in general slightly lower compared to the previous measurements in the Helsinki area (12–13%, Teinilä et al., 2019; Barreira et al., 2021). Higher contribution of sulfate (16–33%) during LRT episodes has been presented in the observations conducted in the years 1999–2007 (Niemi et al., 2009), which may indicate the reduction of SO_2 emissions in recent years (EEA, 2021) and/or that the origins of the air masses were different. The most striking difference between the values presented by Niemi et al. (2009) and the values measured in this study was the fraction of nitrate which was 17–29 times larger in the study by Niemi et al., (2009) than in this work. In Niemi et al., (2009) during LRT events the concentration of nitrate was 1.71 ± 0.60 μg m^{-3} which is over 4 times the average concentration during the cold period (0.39 ± 0.60 μg m^{-3}) and over 11 times the average during the warm period (0.15 ± 0.15 μg m^{-3}) (Table 1). As already mentioned, nitrate was also slightly elevated in PM_1 in the TRA events. The event-type averaged concentrations for the chemical species are presented in the supplement (Table S2).

The air mass back trajectories for the LRT events were studied using NOAA hysplit air mass back trajectories. The trajectories are presented in the supplemental material (Figs. S3–S5). The 72 h back trajectories showed that during the LRT events, the air masses came from central and eastern Europe or the Baltics. These are typical source regions for LRT in southern Finland (Niemi et al., 2009). Sometimes the air masses came over the Baltic Sea spending a significant amount of time on the northern Baltic, especially in the case of the last event when the fraction of nitrate was the highest (30%). At the Baltic Sea, there is a significant amount of ship traffic that contributes to atmospheric concentrations of particles (Seppälä et al., 2021) and NO_x (Jonson et al., 2019; Stipa et al., 2009). NO_2 is converted to nitric acid at a rate of 5% per hour and therefore has a lifetime of approximately 24 h (Geels et al., 2012). The aged exhaust from ship traffic could explain part of the high nitrate fraction in measured particulate matter in these events. The rest of the particulate nitrate is likely to be caused by land-based emissions, such as traffic, energy production, and industry. The fraction of BC in PM_1 was slightly higher compared to BC fractions during the LRT events presented in other studies, 9% (Aurela et al., 2015) and 4.1–6.3% (Niemi et al., 2009) for the aged aerosol (LRT) at the residential site. However, the contribution of land-based traffic may have been lower than usual because of the COVID-19 restrictions.

3.5. Number size distributions of fresh and aged wood-burning events

The WB events likely contain influences from different types of wood-burning emissions as the standard deviation of observed NSDs was large (Fig. 3a). Therefore, individual WB events were analyzed in more detail to investigate if they were related to fresh or aged wood-burning emissions. The organics to BC -ratio (Org/BC -ratio) can be used to estimate the relative age of emissions as BC is emitted directly from the source (primary emission) as a result of incomplete combustion, whereas organic matter is also formed via secondary aerosol formation in the atmosphere. In the atmospheric studies, the highest OC/EC -ratios (up to 25–35) have been typically seen for aged particles, whereas the lowest ratios (approx. 1) have been observed for fresh emissions (Aurela et al., 2011; Timonen et al., 2014; Querol et al., 2013; Karanasiou et al., 2020). In Fig. 5 the WB events have been separated into two categories based on Org/BC -ratios to differentiate between fresh and aged wood-burning emissions. The division point between fresh and aged (or insufficient and efficient burning) was set to the average Org/BC -ratio of 2.2. For the average of all WB event data, the Org/BC -ratio was 1.6, but when the ratio was calculated separately for each event, the ratio was 2.2. This indicates that the ratio was significantly larger for the events with higher concentrations that dominate the averaging. Hereafter, events with an Org/BC -ratio above and below 2.2 are referred to as aged WB and fresh WB events, respectively.

The NSDs of fresh and aged WB events were found to be different (Fig. 5). While the fresh and aged WB events had similar GMD and GSD values (56 nm and 2.0, and 55 nm and 2.0, respectively), the modes were slightly different being 40 nm for fresh and 46 nm for aged WB. However, the aged WB also had another local mode at 23 nm, therefore being strongly bimodal. The GMD of the NSDs remained similar even as the mode changed because in the case of aged WB there were elevated concentrations at the lowest particle sizes. This might be related directly to wood-burning or it may be related to homogenous particle nucleation in aging WB aerosol. In general, particle concentrations during aged WB events were lower and showed less variation in all particle sizes. This was likely because of the higher dilution ratio caused by the higher age of the emissions (Fig. 5). The larger particle size of the aged emissions is expected due to atmospheric processes (such as coagulation, condensation, and secondary aerosol formation processes) that increase the particle size gradually during atmospheric aging. The shape of fresh wood-burning size distribution is very similar to the size distribution observed for birch burning on a stove by Hedberg et al. (2002).

In Fig. 5 the difference in NSDs of fresh and aged WB events was likely a result of both the aging of wood-burning emissions and the stage of the combustion during which the particles were formed. For example, the smoldering conditions (insufficient burning) have been reported to produce larger particles in wood-burning (Ordou and Agranovski, 2019;

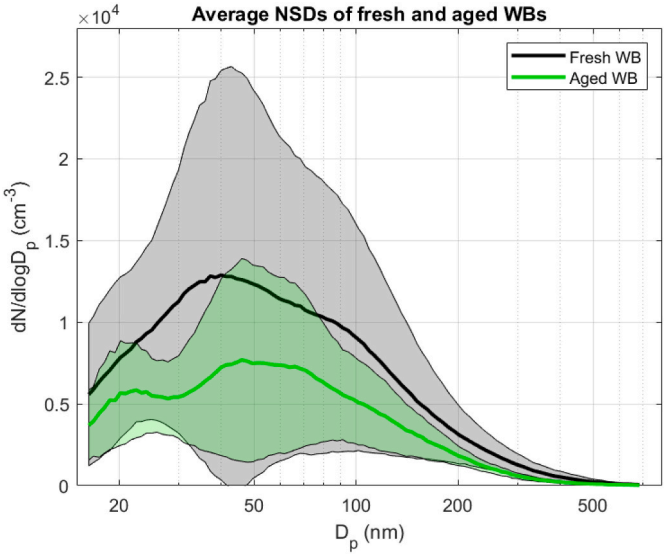

Fig. 5. The average number size distributions (NSD) of fresh (12 events) and aged (8 events) WB events. Average size distributions have been marked with bold lines and light-colored areas display standard deviations.

Tissari et al., 2008). Note that the phase of combustion may also have a large effect on Org/BC -ratio that was used here to separate fresh and aged WB. More BC is formed in efficient flaming burning, whereas in insufficient burning or smoldering a wide range of organic compounds are emitted into the atmosphere. Hence Org/BC -ratio in efficient burning is lower and the ratio in insufficient burning is higher (Khalil and Rasmussen, 2003; Saarnio et al., 2010).

4. Summary and conclusions

This study investigated particle number size distributions for four different prevailing particle sources in the suburban detached housing area. The studied aerosol types were wood-burning, traffic, secondary biogenic, and long-range transport aerosol.

Particle size distributions from studied sources showed noticeable differences. The largest particle GMD was measured for LRT (69 nm) followed by BIO (62 nm), WB (56 nm), and TRA (41 nm), with the modes of 69, 69, 43, and 25 nm, respectively. The observed larger size of LRT and BIO particles was likely due to particle growth during the aging in the atmosphere. Regarding the local primary particle sources, WB had a larger particle size than TRA. WB particles were also showing the largest variability in the NSD. Therefore, the WB events were further separated into two categories, aged and fresh WB events, based on the organics to BC ratio. In addition to the age of the emissions, also the burning conditions (efficient or insufficient burning) and fuel were likely to contribute to the large variability of the WB event NSD.

PM_1 concentration and chemical composition varied between the event types. WB consisted mostly of organics (55%) and BC (34%), whereas TRA was composed of 39% organics, 33% BC, and 16% of nitrate with minor contributions from other sources. BIO was dominated by organics (81%) while LRT had significant contributions of both inorganics (26% nitrate, 12% ammonium, and 10% sulfate) and organics (38%).

Number size distributions investigated systematically for particles associated with different sources in ambient air are scarce in scientific literature. Therefore, increasing the knowledge of source-specific size distributions combined with composition data is needed to better understand the health and climate effects of particles from various sources. Currently, the world is going through climate change and the war in Ukraine has caused fossil fuel prices to reach record highs. These two factors have caused an imminent crisis for energy production that is likely to accelerate changes away from fossil fuels. Additionally to reach the climate goals of societies, in many scenarios the use of fossil fuel combustion is expected to decrease and the use of biomass fuels to increase in the future (Rogelj et al., 2018). The emissions from vehicular traffic (e.g BC) have already been noticed to decrease due to technological advancements and emission legislation (Luoma et al., 2021; Pirjola et al., 2016). However, the regulation of residential combustion emissions is still in its infancy in many European countries (Klimont et al., 2017; Kukkonen et al., 2020).

In this study, the particle size distributions were found to be dependent on the prevailing source possessing different shapes and modal structures, and therefore likely having varying effects on the environment and human health. For example, 5 nm primary particles are shown to translocate from the lungs ending up in urine more efficiently compared to 30 nm particles (Miller et al., 2017), and therefore smaller particles might have more pronounced health effects. Traffic was observed to produce the highest fraction of small particles. In contrast, particles under 40 nm need unrealistically high supersaturations in the atmosphere to act as cloud condensation nuclei and therefore do not contribute to cloud condensation, whereas particles above 120 nm are activated in a wide range of supersaturations (Dusek et al., 2006). In this regard, the effects of fresh traffic emissions on cloud condensation are limited, but as the aerosol ages e.g. during long-range or regional transport (LRT and BIO), the particle size shifts to larger particle sizes and starts to contribute to cloud condensation. In terms of wood-burning, the shape and concentration of wood-burning particles vary significantly between different fuels, burning stages, and device types, and therefore the health and climate effects might vary significantly depending on the site. This variation may also be due to a lack of regulations and after-treatment devices for wood-burning devices.

In addition, the timing of the measurement period allowed us to investigate the effects of the COVID-19 restrictions on the atmospheric particle and gas concentrations. By comparing the period of COVID-19 restrictions to the period before restrictions, the most notable effect was a reduction of NO_x concentrations due to the decrease in traffic volumes during workdays in spring 2020 due to the COVID-19 restrictions.

CRediT authorship contribution statement

Sami D. Harni: handled the, Formal analysis, Software, and, Visualization, and, Writing – original draft, the article. **Sanna Saarikoski:** Writing – review & editing, the article. **Joel Kuula:** Writing – review & editing, the article. **Aku Helin:** Data curation. **Minna Aurela:** Writing – review & editing, the article, Data curation. **Jarkko V. Niemi:** Writing – review & editing, the article. **Anu Kousa:** Data curation. **Topi Rönkkö:** Writing – review & editing, the article. **Hilkka Timonen:** acted as a, Supervision, and, Writing – review & editing, the article.

Declaration of competing interest

The authors declare that they have no known competing financial interests or personal relationships that could have appeared to influence the work reported in this paper.

Data availability

Data will be made available on request.

Acknowledgments

Financial support from Black Carbon Footprint project funded by Business Finland (Grant 528/31/2019) and participating companies, from European Union Horizon 2020 research and innovation programme under grant agreement No 814978 (TUBE), and Grant agreement No 101036245 (RI-URBANS), and from European Regional Development Fund, Urban innovative actions initiative (HOPE; Healthy Outdoor Premises for Everyone, project nro: UIA03-240), Urban Air Quality 2.0 project funded by Technology Industries of Finland Centennial Foundation and by the Academy of Finland via the project Black and Brown Carbon in the Atmosphere and the Cryosphere (BBrCAC) (decision nr. 341271) is gratefully acknowledged. Support and training provided by COST Action CA16109 COLOSSAL and Academy of Finland Flagship funding (grant no. 337552, 337551) are gratefully acknowledged. The authors gratefully acknowledge the NOAA Air Resources Laboratory (ARL) for the provision of the HYSPLIT transport and dispersion model and/or READY website (https://www.ready.noaa.gov) used in this publication.

Appendix A. Supplementary data

Supplementary data to this article can be found online at https://doi.org/10.1016/j.atmosenv.2022.119419.

References

Artaxo, P., Hansson, H.C., 1995. Size distribution of biogenic aerosol particles from the amazon basin. Atmos. Environ. 29, 393–402. https://doi.org/10.1016/1352-2310(94)00178-N.

Aurela, M., Saarikoski, S., Timonen, H., Aalto, P., Keronen, P., Saarnio, K., Teinilä, K., Kulmala, M., Hillamo, R., 2011. Carbonaceous aerosol at a forested and an urban

background sites in Southern Finland. Atmos. Environ. 45, 1394–1401. https://doi.org/10.1016/j.atmosenv.2010.12.039.
Aurela, M., Saarikoski, S., Niemi, J.V., Canonaco, F., Prevot, A.S.H., Frey, A., Carbone, S., Kousa, A., Hillamo, R., 2015. Chemical and source characterization of submicron particles at residential and traffic sites in the Helsinki Metropolitan Area, Finland. Aerosol Air Qual. Res. 15, 1213–1226. https://doi.org/10.4209/aaqr.2014.11.0279.
Bar, S., Parida, B.R., Mandal, S.P., Pandey, A.C., Kumar, N., Mishra, B., 2021. Impacts of partial to complete COVID-19 lockdown on NO2 and PM2.5 levels in major urban cities of Europe and USA. Cities 117, 103308. https://doi.org/10.1016/j.cities.2021.103308.
Barreira, L.M.F., Helin, A., Aurela, M., Teinilä, K., Friman, M., Kangas, L., Niemi, J.V., Portin, H., Kousa, A., Pirjola, L., Rönkkö, T., Saarikoski, S., Timonen, H., 2021. In-depth characterization of submicron particulate matter inter-annual variations at a street canyon site in Northern Europe. Atmos. Chem. Phys. 21, 6297–6314. https://doi.org/10.5194/acp-21-6297.
Birmili, W., Alaviippola, B., Hinneburg, D., Knoth, O., Tuch, T., Borken-Kleefeld, J., Schacht, A., 2009. Dispersion of traffic-related exhaust particles near the Berlin urban motorway – estimation of fleet emission factors. Atmos. Chem. Phys. 9, 2355–2374. https://doi.org/10.5194/acp-9-2355-2009.
Birmili, W., Harrison, R.M., 2008. Fingerprinting particle origins according to their size distribution at a UK rural site. J. Geophys. Res. 113, 1–15. https://doi.org/10.1029/2007JD008562.
Charron, A., Polo-Rehn, L., Besombes, J.L., Golly, B., Buisson, C., Chanut, H., Marchand, N., Guillaud, G., Jaffrezo, J.L., 2019. Identification and quantification of particulate tracers of exhaust and non-exhaust vehicle emissions. Atmos. Chem. Phys. 19, 5187–5207. https://doi.org/10.5194/acp-19-5187-2019.
Chen, Gang, Canonaco, Francesco, Tobler, Anna, Aas, Wenche, Alastuey, Andres, Allan, James, Atabakhsh, Samira, Aurela, Minna, Baltensperger, Urs, Bougiatioti, Aikaterini, De Brito, Joel F., Ceburnis, Darius, Chazeau, Benjamin, Chebaicheb, Hasna, Daellenbach, Kaspar R., Ehn, Mikael, El Haddad, Imad, Eleftheriais, Konstantinos, Favez, Olivier, Flentje, Harald, Font, Anna, Fossum, Kirsten, Freney, Evelyn, Gini, Maria, Green, David C, Heikkinen, Liine, Herrmann, Hartmut, Kalogridis, Athina-Cerise, Keernik, Hannes, Lhotka, Radek, Lin, Chunshui, Lunder, Chris, Maasikmets, Marek, Manousakas, Manousos I., Marchand, Nicolas, Marin, Cristina, Marmurenau, Luminita, Mihalopoulos, Nikolaos, Močnik, Griša, Nęcki, Jaroslaw, O'Dowd, Colin, Ovadnevaite, Jurgita, Thomas, Peter, Jean-Eudes, Petit, Pikridas, Michael, Stephen Matthew, Platt, Pokorná, Petra, Poulain, Laurent, Priestman, Max, Riffault, Véronique, Rinaldi, Matteo, Różański, Kazimierz, Schwarz, Jaroslav, Sciare, Jean, Simon, Leïla, Skiba, Alicja, Slowik, Jay G., Sosedova, Yulia, Stavroulas, Iasonas, Styszko, Katarzyna, Teinemaa, Erik, Timonen, Hilkka, Tremper, Anja, Vasilescu, Jeni, Marta, Via, Vodička, Petro, Wiedensohler, Alfred, Zografou, Olga, Minguillón, María Cruz, Prévôt, André S.H., 2022. European aerosol phenomenology – 8: Harmonised source apportionment of organic aerosol using 22 Year-long ACSM/AMS datasets. Environ. Intern. 166, 107325 https://doi.org/10.1016/j.envint.2022.107325.
Corrigan, A.L., Russell, L.M., Takahama, S., Äijälä, M., Ehn, M., Junninen, H., Rinne, J., Petäjä, T., Kulmala, M., Vogel, A.L., Hoffmann, T., Ebben, C.J., Geiger, F.M., Chhabra, P., Seinfeld, J.H., Worsnop, D.R., Song, W., Auld, J., Williams, J., 2013. Biogenic and biomass burning organic aerosol in a boreal forest at Hyytiälä, Finland, during HUMPPA-COPEC 2010. Atmos. Chem. Phys. 13, 12233–12256. https://doi.org/10.5194/acp-13-12233-2013.
De Filippo, A., Maricq, M.M., 2008. Diesel nucleation mode particles: semivolatile or solid? Environ. Sci. Technol. 42, 7957–796210, 1021/es8010332.
Drinovec, L., Močnik, G., Zotter, P., Prévôt, A.S.H., Ruckstuhl, C., Coz, E., Rupakheti, M., Sciare, J., Müller, T., Wiedensohler, A., Hansen, A.D.A., 2015. The "dual-spot" Aethalometer: an improved measurement of aerosol black carbon with real-time loading compensation. Atmos. Meas. Tech. 8, 965–1979. 10.5194/amt-8-1965-2015.
Dusek, U., Frank, G.P., Hildebrandt, L., Curtius, J., Schneider, J., Walter, S., Chand, D., Drewnick, F., Hings, S., Jung, D., Borrmann, S., Andreae, M.O., 2006. Size matters more than chemistry for cloud-nucleating ability of aerosol particles. Science 312, 1375–1378. https://doi.org/10.1126/science.1125261.
EEA. Air quality in Europe 2021 report, Sources and emissions of air pollutants in Europe, 17th Jan 2022. https://www.eea.europa.eu/publications/air-quality-in-europe-2021/sources-and-emissions-of-air.
Enroth, J., Saarikoski, S., Niemi, J.V., Kousa, A., Ježek, I., Močnik, G., Carbone, S., Kuuluvainen, H., Rönkkö, T., Hillamo, R., Pirjola, L., 2016. Chemical and physical characterization of traffic particles in four different highway environments in the Helsinki metropolitan area. Atmos. Chem. Phys. 16, 5497–5512. https://doi.org/10.5194/acp-16-5497.2016.
Finnish Trasport Infrastructure Agency. Finnish Trasport infrastructure agency (liikennevirasto): liikennemääräkartat, 1st Dec 2020. https://julkinen.vayla.fi/webgis-sovellukset/webgis/template.html?config=liikenne.
Fröhlich, R., Cubison, M.J., Slowik, J.G., Bukowiecki, N., Prévôt, A.S.H., Baltensperger, U., Schneider, J., Kimmel, J.R., Gonin, M., Rohner, U., Worsnop, D.R., Jayne, J.T., 2013. The ToF-ACSM: a portable aerosol chemical speciation monitor with TOFMS detection. Atmos. Meas. Tech. 6, 3225–3241. https://doi.org/10.5194/amt-6-3225-2013.
Gani, S., Bhandari, S., Seraj, S., Wang, D.S., Patel, K., Soni, P., Arub, Z., Habib, G., Hildebrandt, R.L., Apte, J.S., 2019. Submicron aerosol composition in the world's most polluted megacity: the Delhi Aerosol Supersite study. Atmos. Chem. Phys. 19, 6843–6859. https://doi.org/10.5194/acp-19-6843-2019.
Geels, C., Hansen, K.M., Christensen, J.H., Ambelas, S.C., Ellermann, T., Hedegaard, G.B., Hertel, O., Frohn, L.M., Gross, A., Brandt, J., 2012. Projected change in atmospheric nitrogen deposition to the Baltic Sea towards 2020. Atmos. Chem. Phys. 12, 2615–2629. https://doi.org/10.5194/acp-12-2615-2012.
Hedberg, E., Kristensson, A., Ohlsson, M., Johansson, C., Johansson, P.-Å., Swietlicki, E., Vesely, V., Wideqvist, U., Westerholm, R., 2002. Chemical and physical characterization of emissions from birch wood combustion in a wood stove. Atmos. Environ. 36, 4823–4837. https://doi.org/10.1016/S1352-2310(02)00417-x.
Heikkilä, J., Virtanen, A., Rönkkö, T., Keskinen, J., Aakko-Saksa, P., Murtonen, T., 2009. Nanoparticle emissions from a heavy-duty engine running on alternative diesel fuels. Environ. Sci. Technol. 43, 9501–9506. https://doi.org/10.1021/es9013807.
Helin, A., Niemi, J.V., Virkkula, A., Pirjola, L., Teinilä, K., Backman, J., Aurela, M., Saarikoski, S., Rönkkö, T., Asmi, E., Timonen, H., 2018. Characteristics and source apportionment of black carbon in the Helsinki metropolitan area. Finland. Atmos. Environ. 190, 87–98. https://doi.org/10.1016/j.atmosenv.2018.07.022.
Hering, S.V., Kreisberg, N.M., Stolzenburg, M.R., Lewis, G.S., 2007. Comparison of particle size distributions at urban and agricultural sites in California's san joaquin valley. Aerosol Sci. Technol. 41, 86–96. https://doi.org/10.1080/02786820601113290.
Heyder, J., 2004. Deposition of inhaled particles in the human respiratory tract and consequences for regional targeting in respiratory drug delivery. Proc. Am. Thorac. Soc. 1, 315–320. https://doi.org/10.1513/pats.200409-046TA.
Hietikko, R., Kuuluvainen, H., Harrison, R.M., Portin, H., Timonen, H., Niemi, J.V., Rönkkö, T., 2018. Diurnal variation of nanocluster aerosol concentrations and emission factors in a street canyon. Atmos. Environ. 189, 98–106. https://doi.org/10.1016/j.atmosenv.2018.06.031.
Hopke, P.K., Feng, Y., Dai, Q., 2022. Source apportionment of particle number concentrations: a global review. Sci. Total Environ. 819, 153104 https://doi.org/10.1016/j.scitotenv.2022.153104.
Hoppel, W.A., 1978. Determination of aerosol size distribution from the mobility distribution of the charged fraction of aerosols. J. Aerosol Sci. 9, 41–54. https://doi.org/10.1016/0021-8502(78)90062-9.
Hosseini, S., Li, Q., Cocke, D., Weise, D., Miller, A., Shrivastava, M., Miller, J.W., Malingam, S., Princevac, M., Jung, H., 2010. Particle size distributions from laboratory-scale biomass fires using fast response instruments. Atmos. Chem. Phys. 10, 8065–8076. 10.5194/acp-10-8065-2010.
Hovorka, J., Pokorná, P., Hopke, P.K., Křůmal, K., Mikuška, P., Píšová, M., 2015. Wood combustion, a dominant source of winter aerosol in residential district in proximity to a large automobile factory in Central Europe. Atmos. Environ. 113, 98–107. https://doi.org/10.1016/j.atmosenv.2015.04.068.
Hussein, T., Mølgaard, B., Hannuniemi, H., Martikainen, J., Järvi, L., Wegner, T., Ripamonti, G., Weber, S., Vesala, T., Hämeri, K., 2014. Fingerprints of the urban particle number size distribution in Helsinki, Finland: local versus regional characteristics. Boreal Environ. Res. 19, 1–20. http://hdl.handle.net/10138/165162.
ICRP, 1994. Human respiratory tract modle for radiological protection. ICRP (Int. Comm. Radiol. Prot.) Publ. 66 (24), 1–3.
Jonson, J.E., Gauss, M., Jalkanen, J.-P., Johansson, L., 2019. Effects of strengthening the Baltic Sea ECA regulations. Atmos. Chem. Phys. 19, 13469–13487. https://doi.org/10.5194/acp-19-13469-2019.
Karanasiou, A., Panteliadis, P., Perez, N., Minguillón, M.C., Pandolfi, M., Titos, G., Viana, M., Moreno, T., Querol, X., Alastuey, A., 2020. Evaluation of the Semi-continuous OCEC Analyzer Performance with the EUSAAR2 Protocol, vol. 747, 141266. https://doi.org/10.1016/j.scitotenv.2020.141266.
Karjalainen, P., Pirjola, L., Heikkilä, J., Lähde, T., Tzamkiozis, T., Ntziachristos, L., Keskinen, J., Rönkkö, T., 2014. Exhaust particles of modern gasoline vehicles: a laboratory and an on-road study. Atmos. Environ. 97, 262–270. https://doi.org/10.1016/j.atmosenv.2014.08.025.
Khalil, M.A.K., Rasmussen, R.A., 2003. Tracers of wood smoke, Atmos. Environ. Times 37, 1211–1222. https://doi.org/10.1016/S1352-2310(02)01014-2.
Kim, M.J., 2019. Sensitivity of nitrate aerosol production to vehicular emissions in an urban street. Atmosphere 10, 212. 10.3390/atmos10040212.
Kittelson, D.B., Watts, W.F., Johnson, J.P., 2006. On-road and laboratory evaluation of combustion aerosols-Part1: summary of diesel engine results. J. Aerosol Sci. 37, 913–930. https://doi.org/10.1016/j.jaerosci.2005.08.005.
Klimont, Z., Kupiainen, K., Heyes, C., Purohit, P., Cofala, J., Rafaj, P., Borken-Kleefeld, J., Schöpp, W., 2017. Global anthropogenic emissions of particulate matter including black carbon. Atmos. Chem. Phys. 17, 8681–8723. https://doi.org/10.5194/acp-17-8681-2017.
Krecl, P., Ström, J., Johansson, C., 2008. Diurnal variation of atmospheric aerosol during the wood combustion season in Northern Sweden, Atmos. Environ. Times 42, 4113–4125. https://doi.org/10.1016/j.atmosenv.2008.01.026.
Kukkonen, J., López-Aparicio, S., Segersson, D., Geels, C., Kangas, L., Kauhaniemi, M., Maragkidou, A., Jensen, A., Assmuth, T., Karppinen, A., Sofiev, M., Hellén, H., Riikonen, K., Nikmo, J., Kousa, A., Niemi, J.V., Karvosenoja, N., Santos, G.S., Sundvor, I., Im, U., Christensen, J.H., Nielsen, O.-K., Plejdrup, M.S., Nøjgaard, J.K., Omstedt, G., Andersson, C., Forsberg, B., Brandt, J., 2020. The influence of residential wood combustion on the concentrations of $PM_{2.5}$ in four Nordic cities. Atmos. Chem. Phys. 20, 4333–4365. https://doi.org/10.5194/acp-20-4333-2020.
Kulmala, M., 2003. How particles nucleate and grow. Atmos. Sci. 302, 1000–1001. https://doi.org/10.1126/science.1090848.
Kuula, J., Friman, M., Helin, A., Niemi, J.V., Aurela, M., Timonen, H., Saarikoski, S., 2020. Utilization of scattering and absorption-based particulate matter sensors in the environment impacted by residential wood combustion. J. Aerosol Sci. 150, 105671 https://doi.org/10.1016/j.jaerosci.2020.105671.
Kuuluvainen, H., Karjalainen, P., Saukko, E., Ovaska, T., Sirviö, K., Honkanen, M., Olin, M., Niemi, S., Keskinen, J., Rönkkö, T., 2020. Nonvolatile ultrafine particles observed to form trimodal size distributions in non-road diesel engine exhaust. Aerosol Sci. Technol. 54, 1345–1358. https://doi.org/10.1080/02786826.2020.1783432.

Kwon, Hyouk-Soo, Ryu, Min Hyung, Carlsten, Christopher, 2020. Ultrafine particles: unique physicochemical properties relevant to health and disease. Experim. Molecul. Med. 52, 318–320. https://doi.org/10.1038/s12276-020-0405-1.

Liu, Q., Malarvizhi, A.S., Liu, W., Xu, H., Harris, J.T., Yang, J., Duffy, D.Q., Little, M.M., Sha, D., Hai, L., Yang, Y., 2021. Spatiotemporal changes in global nitrogen dioxide emission due to COVID-19 mitigation policies. Sci. Total Environ. 776, 146027 https://doi.org/10.1016/j.scitotenv.2021.146027.

Luoma, K., Niemi, J.V., Aurela, M., Fung, P.L., Helin, A., Hussein, T., Kangas, L., Kousa, A., Rönkkö, T., Timonen, H., Virkkula, A., Petäjä, T., 2021. Spatiotemporal variation and trends in equivalent black carbon in the Helsinki metropolitan area in Finland. Atmos. Chem. Phys. 21, 1173–1189. https://doi.org/10.5194/acp-21-1173-2021.

Mahilang, M., Deb, M.K., Pervez, S., 2021. Biogenic secondary organic aerosols: a review of information mechanism, analytical challenges and environmental impacts. Chemosphere 262. https://doi.org/10.1016/j.chemosphere.2020.127771.

Miller, M.R., Raftis, J.B., Langrish, J.P., McLean, S.G., Samutrtai, P., Connel, S.P., Wilson, S., Vesey, A.T., Fokkens, P.H.B., Boere, A.J.F., Krystek, P., Campell, C.J., Hadoke, P.W.F., Donaldson, K., Cassee, F.R., Newby, D.E., Duffin, R., Mills, N.L., 2017. Inhaled nanoparticles accumulate at sites of vascular disease. ACS Nano 11, 4542–4552. https://doi.org/10.1021/acsnano.6b08551.

Mustafa, B.G., Kia, H., Andrews, G.E., Phylaktou, R., Li, H., 2017. Particle size distribution during pine wood combustion on a cone calorimeter. Proceedings of the Cambridge Particles Meeting, University of Cambridge.

Niemi, J.V., Saarikoski, S., Aurela, M., Tervahattu, H., Hillamo, R., Westphal, D.L., Aarnio, P., Koskentalo, T., Makkonen, U., Vehkamäki, H., Kulmala, M., 2009. Long-range transport episodes of fine particles in southern Finland during 1999-2007. Atmos. Environ. 43, 1255–1264. https://doi.org/10.1016/j.atmosenv.2008.11.022.

Ordou, N., Agranovski, I.E., 2019. Contribution of fine particles to air emission at different phases of biomass burning. Atmosphere 10. https://doi.org/10.3390/atmos10050278.

Petäjä, T., Tabakova, K., Manninen, A., Ezhova, E., O'Connor, E., Moisseev, D., Sinclair, V.A., Backman, J., Levula, J., Luoma, K., Virkkula, A., Paramonov, M., Räty, M., Äijälä, M., Heikkinen, L., Ehn, M., Sipilä, M., Yli-Juuti, T., Virtanen, A., Ritsche, M., Hickmon, N., Pulik, G., Rosenfeld, D., Worsnop, D.R., Bäck, J., Kulmala, M., Kerminen, K.-M., 2022. Influence of biogenic emissions from boreal forests on aerosol–cloud interactions. Nat. Geosci. 15, 42–47. https://doi.org/10.1038/s41561-021-00876-0.

Pirjola, L., Dittrich, A., Niemi, J.V., Saarikoski, S., Timonen, H., Kuuluvainen, H., Järvinen, A., Kousa, A., Rönkkö, T., Hillamo, R., 2016. Physical and chemical characterization of real world particle number and mass emissions from city busses in Finland. Environ. Sci. Technol. 50, 294–304. https://doi.org/10.1021/acs.est.5b04105.

Pirjola, L., Niemi, J.V., Saarikoski, S., Aurela, M., Enroth, J., Carbone, S., Saarnio, K., Kuuluvainen, H., Kousa, A., Rönkkö, T., Hillamo, R., 2017. Physical and chemical characterization of urban winter-time aerosols by mobile measurements in Helsinki, Finland. Atmos. Environ. 158, 60–175. https://doi.org/10.1016/j.atmosenv.2017.03.028.

Pósfai, M., Buseck, P.R., 2010. Nature and climate effects of individual tropospheric aerosol particles. Annu. Rev. Earth Planet Sci. 38, 17–43, 10.1146/annurev.earth.031208.100032.

Querol, X., Alastuey, A., Viana, M., Moreno, T., Reche, C., Minguillón, M.C., Ripoll, A., Pandolfi, M., Amato, F., Karanasiou, A., Pérez, N., Pey, J., Cusack, M., Vázquez, R., Plana, F., Dall'Osto, M., de la Rosa, J., Sánchez de la Campa, A., Fernández-Camacho, R., Rodríguez, S., Pio, C., Alados-Arboledas, L., Titos, G., Artíñano, B., Salvador, P., García Dos Santos, S., Fernández Patier, R., 2013. Variability of carbonaceous aerosols in remote, rural, urban and industrial environments in Spain: implications for air quality policy. Atmos. Chem. Phys. 13, 6185–6206. https://doi.org/10.5194/acp-13-6185-2013.

Reyes, F., Ahumada, S., Rojas, F., Oyola, P., Vásquez, Y., Aguilera, C., Henriquez, A.R., Gramsch, E., Kang, C.M., Saarikoski, S., Teinilä, K., Aurela, M., Timonen, H., 2021. Impact of biomass burning on air quality in temuco city, Chile. Aerosol Air Qual. Res. 21, 210110 https://doi.org/10.4209/aaqr.210110.

Rivas, I., Beddows, D.C.S., Amato, F., Green, D.C., Järvi, L., Hueglin, C., Reche, C., Timonen, H., Fuller, G.W., Niemi, J.V., Pérez, N., Aurela, M., Hopke, P.K., Alastuey, A., Kulmala, M., Harrison, R.M., Querol, X., Kelly, F.J., 2020. Source apportionment of particle number size distribution in urban background and traffic stations in four European cities. Environ. Int. 135, 105345 https://doi.org/10.1016/j.envint.2019.105345.

Rogelj, J., Shindell, D., Jiang, K., Fifita, S., Forster, P., Ginzburg, V., Handa, C., Kheshgi, H., Kobayashi, S., Kriegler, E., Mundaca, L., Séférian, R., Vilariño, M.V., 2018. Mitigation pathways compatible with 1.5°C in the context of sustainable development. In: Global Warming of 1.5°C. An IPCC Special Report on the Impacts of Global Warming of 1.5°C above Pre-industrial Levels and Related Global Greenhouse Gas Emission Pathways, in the Context of Strengthening the Global Response to the Threat of Climate Change, Sustainable Development, and Efforts to Eradicate Poverty. Intergovernmental Panel on Climate Change, Geneva, Switzerland, pp. 313–443, 2018.

Rönkkö, T., Kuuluvainen, H., Karjalainen, P., Keskinen, J., Hillamo, R., Niemi, J.V., Pirjola, L., Timonen, H.J., Saarikoski, S., Saukko, E., Järvinen, A., Silvennoinen, H., Rostedt, A., Olin, M., Yli-Ojanperä, J., Nousiainen, P., Kousa, A., Dal Maso, M., 2017. Traffic is a major source of atmospheric nanocluster aerosol. Proc. Natl. Acad. Sci. USA 114, 7549–7554. https://doi.org/10.1073/pnas.1700830114.

Rönkkö, T., Timonen, H., 2019. Overview of sources and characteristics of nanoparticles in urban traffic-influenced areas. J. Alzheim. Dis. 72, 15–28. https://doi.org/10.3233/JAD-190170.

Rönkkö, T., Virtanen, A., Vaaraslahti, K., Kannosto, J., Keskinen, J., Lappi, M., Pirjola, L., 2007. Nucleation mode particles with a nonvolatile core in the exhaust of a heavy duty diesel vehicle. Environ. Sci. Technol. 41, 6384–6389. https://doi.org/10.1021/es0705339.

Saarikoski, S., Niemi, J.V., Aurela, M., Pirjola, L., Kousa, A., Rönkkö, T., Timonen, H., 2021. Sources of black carbon at residential and traffic environments obtained by two source apportionment methods. Atmos. Chem. Phys. 21, 14851–14869. https://doi.org/10.5194/acp-21-14851-2021.

Saarikoski, S., Sillanpää, M., Sofiev, M., Timonen, H., Saarnio, K., Teinilä, K., Karppinen, A., Kukkonen, J., Hillamo, R., 2007. Chemical composition of aerosols during a major biomass burning episode over northern Europe in spring 2006: experimental and modelling assessments. Atmos. Environ. 41, 3577–3589. https://doi.org/10.1016/j.atmosenv.2006.12.053.

Saarikoski, S., Timonen, H., Saarnio, K., Aurela, M., Järvi, L., Keronen, P., Kerminen, V.-M., Hillamo, R., 2008. Sources of organic carbon in fine particulate matter in northern European urban air. Atmos. Chem. Phys. 8, 6281–6295. https://doi.org/10.5194/acp-8-6281-2008.

Saarnio, K., Aurela, M., Timonen, H., Saarikoski, S., Teinilä, K., Mäkelä, T., Sofiev, M., Koskinen, J., Aalto, P.P., Kulmala, M., Kukkojen, J., Hillamo, R., 2010. Chemical composition of fine particles in fresh smoke plumes from boreal wild-land fires in Europe. Sci. Total Environ. 408, 2527–2542. https://doi.org/10.1016/j.scitotenv.2010.03.010.

Saarnio, K., Niemi, J.V., Saarikoski, S., Aurela, M., Timonen, H., Teinilä, K., Myllynen, M., Frey, A., Lamberg, H., Jokiniemi, J., Hillamo, R., 2012. Using monosaccharide anhydrides to estimate the impact of wood combustion on fine particles in the Helsinki Metropolitan Area. Boreal Environ. Res. 17, 163–183. http://hdl.handle.net/10138/165141.

Sandradewi, J., Prévôt, A.S., Szidat, S., Perron, N., Alfarra, M., Lanz, R.V.A., Weingartner, E., Baltensperger, U., 2008. Using aerosol light absorption measurements for the quantitative determination of wood-burning and traffic emission contributions to particulate matter. Environ. Sci. Technol. 42, 3316–3323. https://doi.org/10.1021/es702253m.

Savolahti, M., Karvosenoja, N., Tissari, J., Kupiainen, K., Sippula, O., Jokiniemi, J., 2016. Black carbon and fine particle emissions in Finnish residential wood combustion: emission projections, reduction measures and the impact of combustion practices. Atmos. Environ. 140, 495–505. https://doi.org/10.1016/j.atmosenv.2016.06.023.

Sgro, L.A., Borghese, A., Speranza, L., Barone, A.C., Minutolo, P., Bruno, A., D'Anna, A., D'Alessio, A., 2008. Measurements of nanoparticles of organic carbon and soot in flames and vehicle exhausts. Environ. Sci. Technol. 42, 859–863. https://doi.org/10.1021/es070485s.

Sgro, L.A., Sementa, P., Vaglieco, B.M., Rusciano, G., D'Anna, A., Minutolo, P., 2012. Investigating the origin of nuclei particles in GDI engine exhausts(2012). Combust. Flame 159, 1687–1692. https://doi.org/10.1016/j.combustflame.2011.12.013.

Seppälä, S., Kuula, J., Hyvärinen, A., Saarikoski, S., Rönkkö, T., Jalkanen, J., Timonen, H., 2021. Effects of marine fuel sulfur restrictions on particle number concentrations and size distributions in ship plumes at the Baltic Sea. Atmos. Chem. Phys. 21, 3215–3234. https://doi.org/10.5194/acp-21-3215-2021.

Simoneit, B.R.T., Schauer, J.J., Nolte, C.G., Oros, D.R., Elias, V.O., Fraser, M.P., Rogge, W.F., Cass, G.R., 1999. Levoglucosan, a tracer for cellulose in biomass burning and atmospheric particles. Atmos. Environ. 33, 173–182. https://doi.org/10.1016/S1352-2310(98)00145-9.

Sokhi, R.S., Singh, V., Querol, X., Finardi, S., Targino, A.C., Andrade, M. de F., Pavlovic, R., Garland, R.M., Massagué, J., Kong, s., Baklanov, a., Ren, L., Tarasova, O., Carmichael, G., Peuch, V.-H., Anand, V., Arbilla, G., Badali, K., Beig, G., Belalcazar, L.C., Bolignano, A., Brimblecombe, P., Camacho, P., Casallas, A., Charland, J.-P., Choi, J., Chourdakis, R., Coll, I., Collins, M., Cyrys, J., da Silva, C.M., Di Giosa, A.D., Di Leo, A., Ferro, C., Gavidia-Calderon, M., Gayen, A., Ginzburg, A., Godefroy, F., Gonzalez, Y.A., Guevara-Luna, M., M Haque, Sk, Havenga, H., Herod, D., Hõrrak, U., Hussein, T., Ibarra, S., Jaimes, M., Kaasik, M., Khaiwal, R., Kim, J., Kousa, A., Kukkonen, J., Kulmala, M., Kuula, J., La Violette, N., Lanzani, G., Liu, X., MacDougall, S., Manseau, P.M., Marchegiani, G., McDonald, B., Mishra, S.V., Molina, L.T., Mooibroek, D., Mor, S., Moussiopoulos, N., Murena, F., Niemi, J.V., Noe, S., Nogueira, T., Norman, M., Pérez-Camaño, J.L., Petäjä, T., Piketh, S., Rathod, A., Reid, K., Retama, A., Rivera, O., Rojas, N.Y., Rojas-Quincho, J.P., San José, R., Sánchez, O., Seguel, R.J., Sillanpää, S., Su, Y., Tapper, N., Terrazas, A., Timonen, H., Toscano, D., Tsegas, G., Velders, G.J.M., Vlachokostas, C., von Schneidemesser, E., Vpm, R., Yadav, R., Zalakeviciute, R., Zavala, M., 2021. A global observational analysis to understand changes in air quality during exceptionally low anthropogenic emission conditions. Environ. Int. 157, 106818 https://doi.org/10.1016/j.envint.2021.106818.

Stein, A.F., Draxler, R.R., Rolph, G.D., Stunder, B.J.B., Cohen, M.D., Ngan, F., 2015. NOAA's HYSPLIT atmospheric transport and dispersion modeling system. Bull. Am. Meteorol. Soc. 96, 2059–2077. https://doi.org/10.1175/BAMS-D-14-00110.1.

Stipa, T., Jalkanen, U.-P., Hongisto, M., Kalli, J., Brink, A., 2009. Emissions of Nox from Baltic Shipping and First Estimates of Their Effects on Air Quality and Eutrophication of the Baltic Sea. http://hdl.handle.net/10138/1209.

Teinilä, K., Aurela, M., Niemi, J.V., Kousa, A., Petäjä, T., Järvi, L., Hillamo, R., Kangas, L., Saarikoski, S., Timonen, H., 2019. Concentration variation of gaseous and particulate pollutants in the Helsinki city center — observations from a two-year campaign from 2013–2015. Boreal Environ. Res. 24, 115–136. http://hdl.handle.net/10138/312715.

Teinilä, K., Timonen, H., Aurela, M., Kuula, J., Rönkkö, T., Hellèn, H., Loukkola, K., Kousa, A., Niemi, J.V., Saarikoski, S., 2022. Characterization of particle sources and comparison of different particle metrics in an urban detached housing area. Finland, Atmos. Environ. 272, 118939 https://doi.org/10.1016/j.atmosenv.2022.118939.

Timonen, H., Jaffe, D.A., Wigder, N., Hee, J., Gao, H., Pitzman, L., Cary, R.A., 2014. Sources of carbonaceous aerosol in the free troposphere. Atmos. Environ. 92, 146–153. https://doi.org/10.1016/j.atmosenv.2014.04.014.

Timonen, H., Mylläri, F., Simonen, P., Aurela, M., Maasikmets, M., Bloss, M., Kupri, H.-L., Vainumäe, K., Lepistö, T., Salo, L., Niemelä, V., Seppälä, S., Jalava, P.I., Teinemaa, E., Saarikoski, S., Rönkkö, T., 2021. Household solid waste combustion with wood increases particulate trace metal and lung depositel surfase area emissions. J. Environ. Manag. 293, 112793 https://doi.org/10.1016/j.jenvman.2021.112793.

Timonen, H., Saarikoski, S., Tolonen-Kivimaki, O., Aurela, M., Saarnio, K., Petaja, T., Aalto, P.P., Kulmala, M., Pakkanen, T., Hillamo, R., 2008. Size distributions, sources and source areas of water-soluble organic carbon in urban background air. Atmos. Chem. Phys. 8, 5635–5647. https://doi.org/10.5194/acp-8-5635-2008.

Tissari, J., Lyyränen, J., Hytönen, K., Sippula, O., Tapper, U., Frey, A., Saarnio, K., Pennanen, A.S., Hillamo, R., Salonen, R.O., Hirvonen, M.R., Jokiniemi, J., 2008. Fine particle and gaseous emissions from normal and smoldering wood combustion in a conventional masonry heater. Atmos. Environ. 42, 7862–7873. https://doi.org/10.1016/j.atmosenv.2008.07.019.

Tiwari, M., Sahu, S.K., Bhangare, R.C., Yousaf, A., Pandit, G.G., 2014. Particle size distributions of ultrafine combustion aerosols generated from household fuels. Atmos. Pollut. Res. 5, 145–150. https://doi.org/10.5094/APR.2014.018.

Torkmahalleh, M.A., Akhmetvaliyeva, Z., Omran, A.D., Omran, F.D., Naseri, M. Kazemitabar Ma, Naseri, Mo, Sharifi, H., Malekipirbazari, M., Adotey, E.K., Gorjinezhad, S., Eghtesadi, N., Sabanov, S., Alastuey, A., Andrade, F.M., Buonanno, G., Carbone, S., Cárdenas-Fuentes, D.E., Cassee, F.R., Dai, Q., Henríquez, A., Hopke, P.K., Keronen, P., Khwaja, H.A., Kim, J., Kulmala, M., Kumar, P., Kushta, J., Kuula, J., Massagué, J., Mitchell, T., Mooibroek, D., Morawska, L., Niemi, J.V., Ngagine, S.H., Norman, M., Oyama, B., Oyola, P., Öztürk, F., Petäjä, T., Querol, X., Rashidi, Y., Reyes, F., Ross-Jones, M., Salthammer, T., Savvides, C., Stabile, L., Sjöberg, K., Söderlund, K., Raman, R.S., Timonen, H., Umezawa, M., Viana, M., Xie, S., 2021. Global air quality and COVID-19 pandemic: do we breathe cleaner air? Aerosol Air Qual. Res. 21, 200567 https://doi.org/10.4209/aaqr.200567.

TSI. Aerosol statistics, lognormal distributions, and dN/dlogDp. available at: http://www.tsi.com/uploadedFiles/Product_Information/Literature/Application_Notes/PR-001-RevA_Aerosol-Statistics-AppNote.pd, 29th Jun 2021.

Twomey, S., 1977. The influence of pollution on the shortwave albedo of cloud. J. Atmos. Sci. 34, 1149–1152.

Vargas, F.A., Rojas, N.Y., Pachon, J.E., Russel, A.G., 2012. PM10 characterization and source apportionment at two residential Areas in Bogota, Amos. Pollut. Res. 3, 72–80. https://doi.org/10.5094/APR.2012.006.

Virtanen, A., Joutsensaari, J., Koop, T., Kannosto, J., Yli-Pirilä, P., Leskinen, J., Mäkelä, J.M., Holopainen, J.K., Pöschl, U., Kulmala, M., Worsnop, D.R., Laaksonen, 2010. An amorphous solid state of biogenic secondary organic aerosol particles. Nature 467, 824–827. https://doi.org/10.1038/nature09455.

Waldén, J., Waldén, T., Laurila, S., Hakola, H.. Demonstration of eqvivalence of PM2.5 and PM10 measurement methods in Kuopio 2014-2015. http://handle.net/10138/173933.

Wardayo, A.Y.P., Morawska, L., Ristovski, Z.D., Marsh, J., 2006. Quantification of particle number and mass emission factors from combustion of queensland trees. Environ. Sci. Technol. 40, 5696–5703. https://doi.org/10.1021/es0609497.

Watson, J.G., Chow, J.C., Park, K., Lowenthal, D.H., 2006. Nanoparticle and ultrafine particle events at the Fresno supersite. J. Air Waste Manag. Assoc. 56, 417–430. https://doi.org/10.1080/10473289.2006.10464526.

Who, 2021. World Health Organization, WHO global air quality guidelines: particulate matter (PM2.5 and PM10), ozone, nitrogen dioxide, sulfur dioxide and carbon monoxide. https://apps.who.int/iris/handle/10665/345329. License: CC BY-NC-SA 3.0 IGO.

Xiao, M., Hoyle, C.R., Dada, L., Stolzenburg, D., Kürten, A., Wang, M., Lamkaddam, H., Garmash, O., Mentler, B., Molteni, U., Baccarini, A., Simon, M., He, X.-C., Lehtipalo, K., Ahonen, L.R., Baalbaki, R., Bauer, P.S., Bell, L. Beck D., Bianchi, F., Brilke, S., Chen, D., Chiu, R., Dias, A., Duplissy, J., Finkenzeller, H., Gordon, H., Hofbauer, V., Kim, C., Koenig, T.K., Lampilahti, J., Lee, C.P., Li, Z., Mai, H., Makhmutov, V., Manninen, H., Marten, R., Mathot, S., Mauldin, R.L., Nie, W., Onnela, A., Partoll, E., Petäjä, T., Pfeifer, J., Pospisilova, V., Quéléver, L.L.J., Rissanen, M., Schobesberger, S., Schuchmann, S., Stozhkov, Y., Tauber, C., Tham, Y. J., Tomé, A., Vazquez-Pufleau, M., Wagner, A.C., Wagner, r., Wang, Y., Weitz, L., Wimmer, D., Wu, Y., Yan, C., Ye, P., Ye, Q., Zha, Q., Zhou, X., Amorim, A., Carslaw, K., Curtius, J., Hansel, A., Volkamer, R., Winkler, P.M., Flagan, R.C., Kulmala, M., Worsnop, D.R., Kirkby, J., Donahue, N.M., Baltensperger, U., Haddad, I.E., Dommen, J., 2021. The drivïng factors of new particle formation and growth in the polluted boundary layer. Atmos. Chem. Phys. 21, 14275–14291. https://doi.org/10.5194/acp-21-14275-2021.

Zheng, Y., Cheng, X., Liao, K., Li, Y., Li, Y.J., Huang, R.-J., Hu, W., Liu, Y., Zhu, t., Chen, S., Zeng, L., Worsnop, D.R., Cheng, Q., 2020. Characterization of anthropogenic organic aerosols by TOF-ACSM with the new capture vaporizer. Atmos. Meas. Tech. 13, 2457–2472. https://doi.org/10.5194/amt-13-2457-2020.

Zhu, Y., Hinds, W.C., Kim, S., Sioutas, C., 2002. Concentration and size distribution of ultrafine particles near a major highway. J. Air Waste Manag. Assoc. 52, 1032–1042. https://doi.org/10.1080/10473289.2002.10470842.

Zhu, W., Luo, L., Cheng, Z., Yan, N., Lou, S., Ma, Y., 2018. Characteristics and contributions of biogenic secondary organic aerosol tracers to PM2.5 in Shanghai, China. Atmos. Pollut. Res. 9, 179–188. https://doi.org/10.1016/j.apr.2017.09.001.

Zotter, B., Herich, H., Gysel, M., El-Haddad, I., Zhang, Y., Močnik, G., Hüglin, C., Baltensperger, U., Szidat, S., Prévôt, A.S.H., 2017. Evaluation of the absorption Ångström exponents for traffic and wood burning in the Aethalometer-based source apportionment using radiocarbon measurements of ambient aerosol. Atmos. Chem. Phys. 17 https://doi.org/10.5194/acp-17-4229-2017, 4249-4249.